nature metabolism

Letter

https://doi.org/10.1038/s42255-023-00815-w

Acarbose suppresses symptoms of mitochondrial disease in a mouse model of Leigh syndrome

Received: 10 January 2022

Accepted: 4 May 2023

Published online: 26 June 2023

Check for updates

A list of authors and their affiliations appears at the end of the paper

Mitochondrial diseases represent a spectrum of disorders caused by impaired mitochondrial function, ranging in severity from mortality during infancy to progressive adult-onset disease. Mitochondrial dysfunction is also recognized as a molecular hallmark of the biological ageing process. Rapamycin, a drug that increases lifespan and health during normative ageing, also increases survival and reduces neurological symptoms in a mouse model of the severe mitochondrial disease Leigh syndrome. The Ndufs4 knockout (*Ndufs4*$^{-/-}$) mouse lacks the complex I subunit NDUFS4 and shows rapid onset and progression of neurodegeneration mimicking patients with Leigh syndrome. Here we show that another drug that extends lifespan and delays normative ageing in mice, acarbose, also suppresses symptoms of disease and improves survival of *Ndufs4*$^{-/-}$ mice. Unlike rapamycin, acarbose rescues disease phenotypes independently of inhibition of the mechanistic target of rapamycin. Furthermore, rapamycin and acarbose have additive effects in delaying neurological symptoms and increasing maximum lifespan in *Ndufs4*$^{-/-}$ mice. We find that acarbose remodels the intestinal microbiome and alters the production of short-chain fatty acids. Supplementation with tributyrin, a source of butyric acid, recapitulates some effects of acarbose on lifespan and disease progression, while depletion of the endogenous microbiome in *Ndufs4*$^{-/-}$ mice appears to fully recapitulate the effects of acarbose on healthspan and lifespan in these animals. To our knowledge, this study provides the first evidence that alteration of the gut microbiome plays a significant role in severe mitochondrial disease and provides further support for the model that biological ageing and severe mitochondrial disorders share underlying common mechanisms.

Mitochondrial disease is a term encompassing numerous disorders characterized by loss of function in one or more mitochondrial processes[1,2]. These mitochondrial dysfunctions affect primarily energy-demanding tissues, such as skeletal muscle, heart and brain, and manifest with different degrees of severity as seizures, myopathies, cardiomyopathies, encephalopathies and cerebellar ataxias. Currently, no known cure or treatment is available for any of these pathologies, and it is estimated that at least 1 in 5,000 live births suffers from severe forms of mitochondrial disease, with crippling consequences for quality of life and extremely reduced life expectancy[3].

Mutations in Complex I (NADH:Ubiquinone Oxidoreductase) of the mitochondrial electron transport chain have been reported

e-mail: kaeber@uw.edu

in up to 30% of paediatric mitochondrial diseases, including severe pathologies such as mitochondrial encephalomyopathy with lactic acidosis and stroke-like episodes (MELAS), fatal infantile lactic acidosis, leukoencephalopathy, neonatal cardiomyopathy and Leigh syndrome, a neurometabolic degenerative disorder which is often fatal in the first 3 yr of life[1,4]. Mutations in the structural subunit of Complex I NADH-Dehydrogenase Ubiquinone Fe-S Protein 4 (NDUFS4) often cause loss of function of the whole complex and have been associated with severe forms of Leigh syndrome[5]. Knockout of exon 2 of the *Ndufs4* gene in mice (*Ndufs4*$^{-/-}$) recapitulates several aspects of Complex I deficiencies, including encephalopathy, retarded growth rate, lethargy, loss of motor skills, lactic acidosis and extremely reduced lifespan[6].

Daily administration of rapamycin, an inhibitor of the nutrient sensing mechanistic target of rapamycin complex I (mTORC1), rescues multiple manifestations of mitochondrial disease in *Ndufs4*$^{-/-}$ mice, including neurological symptoms, accumulation of glycolytic intermediates and lactate, loss of body fat, aberrant nutrient and growth factor signalling, and survival[7,8]. Hyperactivation of mTORC1 has been observed in the brain of *Ndufs4*$^{-/-}$ mice as well as in other models of mitochondrial disease[7,9,10]; however, the precise mechanisms by which rapamycin attenuates mitochondrial dysfunction remain unknown. A metabolic shift away from glycolysis may partially contribute to disease rescue; previous evidence suggests mTORC1 signalling in the liver may contribute[11] to disease rescue, along with inhibition of protein kinase C signalling in the brain[12]. Importantly, there are initial data indicating that rapamycin therapy may improve health in patients suffering from adult-onset MELAS syndrome[13] as well as from paediatric Leigh syndrome[14].

Inhibition of mTORC1 with rapamycin is also a robust intervention for slowing or reversing biological ageing. Rapamycin treatment improves health and increases lifespan during normative ageing across multiple organisms including yeast[15], worms[16], fruit flies[17] and mice[18]. In mice, lifespan extension has been reported in multiple strain backgrounds, across a broad dose range involving both dietary feeding and intraperitoneal injection[18–28]. Age-related phenotypes where rapamycin has been reported to have positive effects include lower incidence of age-related cancers[19,29], protection against age-related cognitive dysfunction[30,31], preservation of tendon[32], improved heart function[33–35], restoration of immune function[36], improved kidney function[37], rejuvenation of oral health[38,39], improved intestinal function and reduced gut dysbiosis[27,40], and preservation of ovarian function[41]. Although early, there is initial evidence suggesting similar effects on the ageing heart in dogs[42] and in immune function in humans[43,44].

Mitochondrial dysfunction is one of the primary hallmarks of ageing[45] which has been implicated in numerous age-related disorders and functional declines[46–48]. While it is clear that severe mitochondrial disease does not clinically resemble accelerated ageing, this connection has led us to hypothesize that ageing is, to some extent, an acquired mitochondrial disease[49]. The observation that mTOR dysregulation is shared between mitochondrial disease and normative ageing can be viewed as support for this hypothesis, as can the fact that rapamycin is among the most effective known interventions at alleviating aspects of both conditions.

To further test the hypothesis that mitochondrial disease and biological ageing share common biological underpinnings, we set out to test whether the drug acarbose could impact disease progression and survival in *Ndufs4*$^{-/-}$ mice. Acarbose is an inhibitor of intestinal alpha-glucosidases and pancreatic alpha-amylases approved for the management of non-insulin-dependent diabetes[50]. Similar to rapamycin, acarbose has also been found to improve health and lifespan in mice[51,52]. Here we report the discovery that acarbose has comparable efficacy to rapamycin at delaying disease progression and increasing survival in *Ndufs4*$^{-/-}$ mice. Unlike rapamycin, acarbose treatment does not inhibit mTOR signalling but instead remodels the intestinal microbiome and alters the production of short-chain fatty acids (SCFAs). Depletion of the endogenous microbiome and butyrate supplementation are sufficient to rescue disease phenotypes, suggesting that (1) acarbose may ameliorate the progression of mitochondrial disease by altering the composition of the intestinal microbiome and (2) the intestinal microbiome is a critical player in the aetiology and progression of neurological mitochondrial disease. Altogether, these results provide further support for the hypothesis that ageing and mitochondrial disorders share common underlying mechanisms and introduce the microbiome as a potential area of intervention to treat severe mitochondrial disease.

Results

Acarbose rescues mitochondrial disease in *Ndufs4*$^{-/-}$ mice

Ndufs4$^{-/-}$ mice older than postnatal (p.n.) day 38 present characteristic brain lesions, including vacuolation in the vestibular nuclei, cerebellar vermis and olfactory bulb; increased vascularity of the brainstem and posterior cerebellum; and widespread astroglial and microglial reactivity[6,53,54]. To determine whether acarbose can mitigate the appearance of these lesions, we fed *Ndufs4*$^{-/-}$ mice with either regular chow or chow containing 1,000 ppm acarbose from weaning (around p.n. day 21) to 50 d of age, when mice were sacrificed. Mice were anaesthetised with a ketamine/xylazine mix and perfused intracardially with PBS and 10% neutral-buffered formalin. Deterioration of mitochondrial function is more prominent in the olfactory bulb, region of the vestibular nuclei of the brainstem and cerebellum of *Ndufs4*$^{-/-}$ brains[54]. To better determine whether acarbose rescues signs of pathology in these regions, we sectioned 10% neutral-buffered formalin-perfused and fixed brains. As expected, untreated *Ndufs4*$^{-/-}$ mice showed extensive vacuolation in the olfactory bulb, vestibular nuclei and cerebellum. Acarbose robustly reduced vacuolation in the olfactory bulb and cerebellum, and showed a trend toward reduced levels of vacuolation in the vestibular nuclei that did not reach statistical significance (Fig. 1a–d). We examined the levels of brain astrogliosis and microgliosis in *Ndufs4*$^{-/-}$ mice and in mice treated with acarbose by performing immunohistochemistry against Glial Fibrillary Acidic Protein (GFAP), a marker of astrocyte activation, and Ionized calcium-binding adapter molecule 1 (Iba1), a marker of microglia activation. As expected, *Ndufs4*$^{-/-}$ mice displayed abundant GFAP and Iba1 immunopositive staining throughout the brain, which was particularly pronounced in the most affected regions (olfactory bulb, cerebellum, vestibular nuclei) (Fig. 1a–f). *Ndufs4*$^{-/-}$ mice showed increased number of microglia in all stages of activation, with increased representation of thick and stout microglial processes (Extended Data Fig. 1a, wider arrows) compared with thin, ramified microglia (Extended Data Fig. 1a, thin arrows) in wild-type animals, consistent with microglial activation. Acarbose significantly reduced GFAP-positive staining in the olfactory bulb and brainstem/vestibular nuclei and reduced Iba1 staining in the olfactory bulb of *Ndufs4*$^{-/-}$ mice (Fig. 1a–c,e,f). These results were also recapitulated by semiquantitative scoring of GFAP and Iba1 immunostaining across multiple brain regions (Extended Data Fig. 1b,c). Lastly, we examined the expression levels of the glial inflammatory marker TREM2 via western blot, but we did not find any significant changes across genotypes or treatments (Extended Data Fig. 1d,e).

Next, we sought to determine whether acarbose could suppress neurological phenotypes displayed by *Ndufs4*$^{-/-}$ mice. We observed mice treated with acarbose daily from p.n. day 21 until death or euthanasia and recorded the initial onset of hind-limb clasping, a characteristic neurological symptom of *Ndufs4*$^{-/-}$ mice[6]. Consistent with the reduction in brain pathology (Fig. 1 and Extended Data Fig. 1), acarbose significantly delayed the onset of clasping by approximately 10 d or 23% (Fig. 2a). Untreated *Ndufs4*$^{-/-}$ mice are growth-impaired and weigh consistently less than wild-type or heterozygous littermates throughout their lifespan (Fig. 2b,c). Additionally, they begin losing weight around 35 d p.n. as neurological symptoms begin to appear (Fig. 2c). Both wild-type and *Ndufs4*$^{-/-}$ mice treated with acarbose showed delayed

https://doi.org/10.1038/s42255-023-00815-w

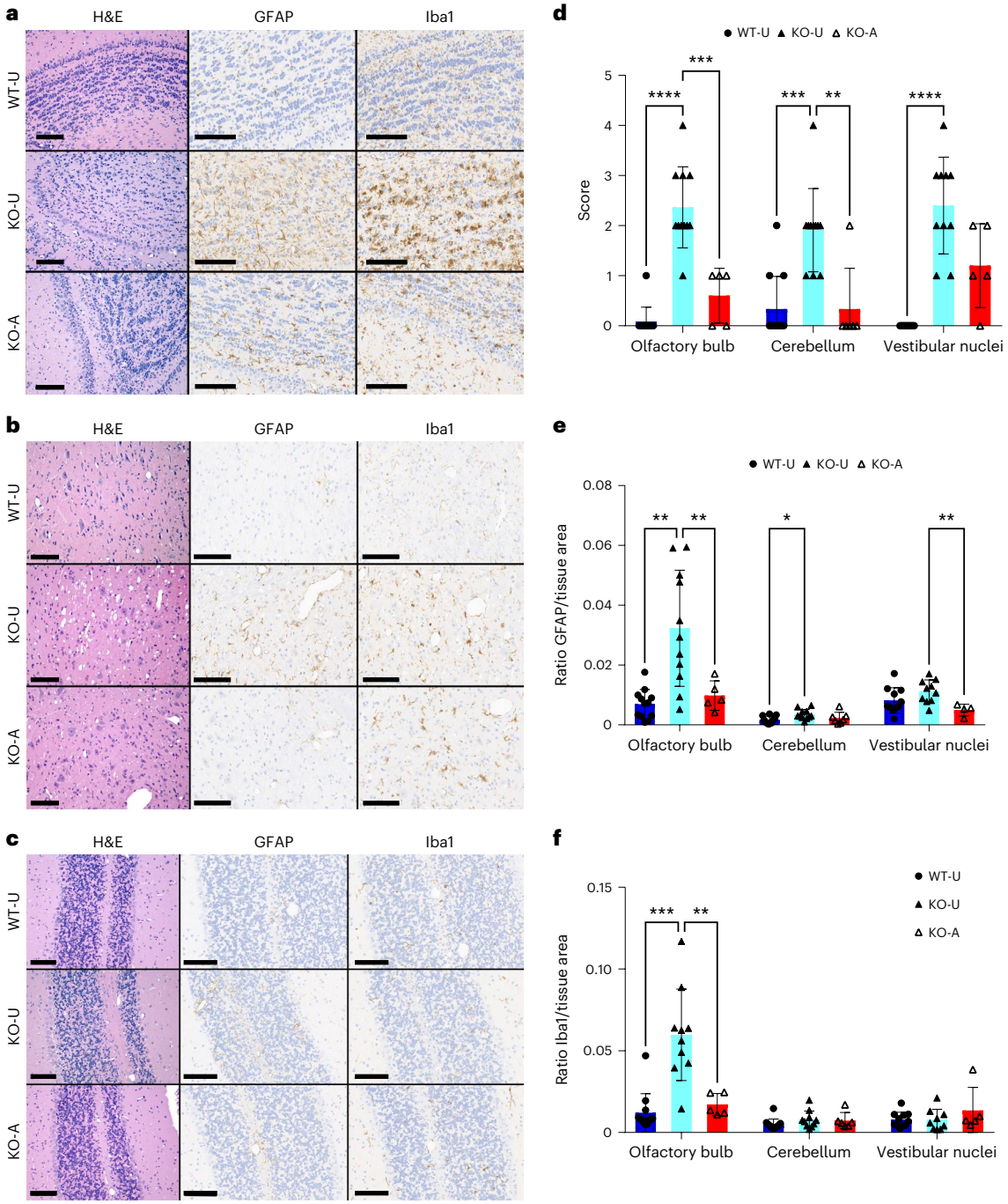

Fig. 1 | Acarbose reduces brain lesions across the brain in *Ndufs4*$^{-/-}$ mice. **a**,**b**,**c**, Representative micrographs of brain sections of the olfactory bulb (**a**), vestibular nuclei (**b**) and cerebellum (**c**) from wild-type untreated (WT-U), *Ndufs4*$^{-/-}$ untreated (KO-U) and *Ndufs4*$^{-/-}$ treated with acarbose (KO-A), stained with H&E, anti-GFAP immunohistochemistry (GFAP) or anti-Iba1 immunohistochemistry. Scale bars, 100 µm. **d**, Vacuolation semiquantitative score in WT-U, KO-U and KO-A mice. Data are presented as individual values (closed circles, WT-U; closed triangles, KO-U; open triangles, KO-A) superimposed on mean ± s.d. $N = 12$ WT-U, $N = 11$ KO-U, $N = 6$ KO-A. Mixed-effect model P values: WT-U versus KO-U, olfactory bulb <0.0001 (mean difference −2.23; 95% confidence interval (95% CI), −2.966 to −1.595), cerebellum 0.0002 (mean difference −1.576; 95% CI, −2.372 to −0.7797), vestibular nuclei <0.0001 (mean difference −2.4; 95% CI, −3.253 to 1.547); KO-U versus KO-A, olfactory bulb 0.0008 (mean difference 1.764; 95% CI, 0.8347 to 2.693), cerebellum 0.0084 (mean difference 1.576; 95% CI, 0.4425 to 2.709). **e**,**f**, Quantitative immunohistochemistry of GFAP (**e**) and Iba1 (**f**) immunohistochemical staining in WT-U, KO-U and KO-A mice. Data are presented as individual values (closed circles, WT-U; closed triangles, KO-U; open triangles, KO-A) superimposed on mean ± s.d. $N = 12$ WT-U, $N = 11$ KO-U, $N = 6$ KO-A. Mixed-effect model P values: WT-U versus KO-U, olfactory bulb 0.0037 (mean difference −0.02538; 95% CI, −0.04159 to −0.009162), cerebellum 0.0236 (mean difference −0.001827; 95% CI, −0.003424 to −0.0002298); KO-U versus KO-A, olfactory bulb 0.0090 (mean difference 0.02250; 95% CI, 0.005900 to 0.03910), vestibular nuclei 0.0056 (mean difference 0.006238; 95% CI, 0.002020 to 0.01046). $N = 12$ WT-U, $N = 11$ KO-U, $N = 7$ KO-A. *$P < 0.05$; **$P < 0.01$; ***$P < 0.001$; ****$P < 0.0001$.

growth compared with their isogenic controls (Fig. 2b,c). *Ndufs4*$^{-/-}$ mice treated with acarbose reached their peak weight around 10 d later than untreated mice (p.n. 47 versus p.n. 37; Fig. 2c). Consistent with the delay in the onset of clasping (Fig. 2a), acarbose-treated animals did not show a similar sharp decline in weight after onset of the disease (Fig. 2c). Lastly, we measured the effect of acarbose on survival and observed a

https://doi.org/10.1038/s42255-023-00815-w

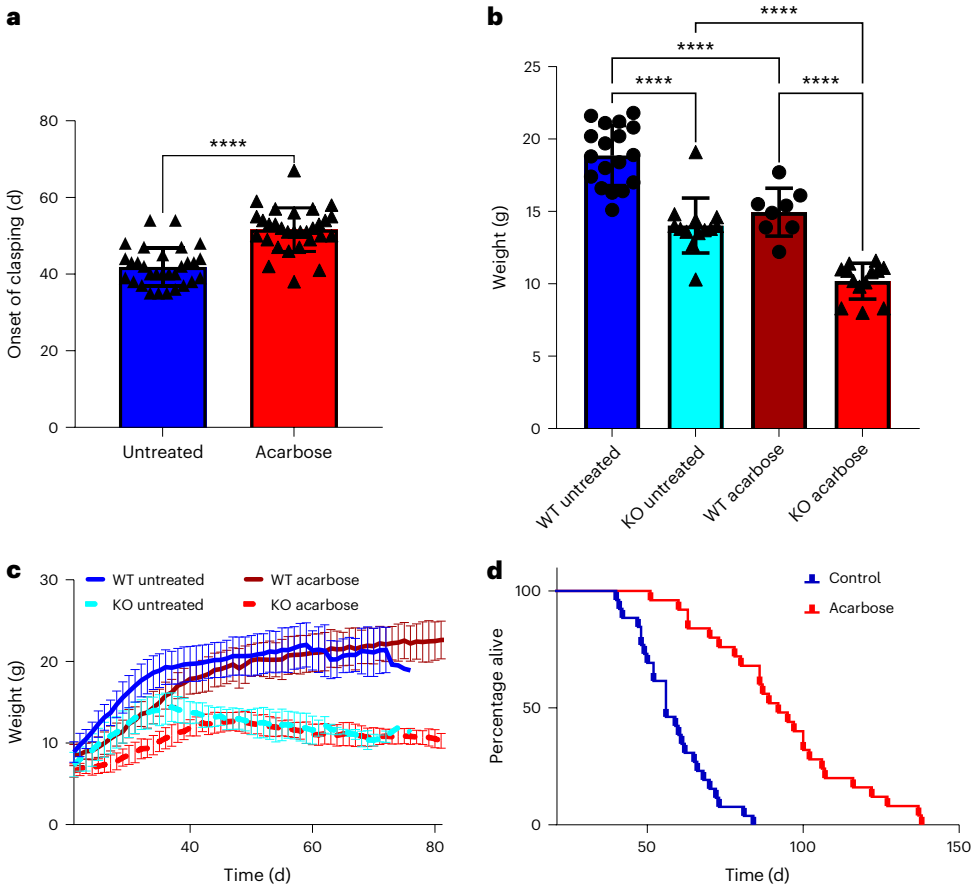

Fig. 2 | Acarbose increases survival and delays onset of disease in *Ndufs4*$^{-/-}$ mice. Wild-type and *Ndufs4*$^{-/-}$ mice were fed either control chow or chow supplemented with 0.1% (1,000 ppm) acarbose from weaning (p.n. day 21). **a**, Onset of neurological symptoms (clasping) measured in days after birth in control-chow (blue)- and acarbose-chow (red)-fed *Ndufs4*$^{-/-}$ mice. Bars are mean ± s.d. ****$P < 0.0001$, two-sided Student's *t*-test. $N = 30$ per group **b**, Comparison of weights at 35 d p.n. for control-chow-fed wild-type (WT untreated) and *Ndufs4*$^{-/-}$ (KO untreated) mice, and acarbose-chow-fed wild-type (WT acarbose) and *Ndufs4*$^{-/-}$ (KO acarbose) mice. Bars are mean ± s.d. ****Adjusted $P < 0.0001$, one-way analysis of variance (ANOVA). $N = 18$ wild-type untreated, $N = 13$ *Ndufs4*$^{-/-}$ untreated, $N = 8$ wild-type acarbose, $N = 15$ *Ndufs4*$^{-/-}$ acarbose, sex: both. **c**, Weight progression from weaning until p.n. day 81. Solid dark blue, wild-type mice fed control chow; solid dark red, wild-type mice fed acarbose chow; dotted light blue, *Ndufs4*$^{-/-}$ mice fed control chow; dotted light red, *Ndufs4*$^{-/-}$ mice fed acarbose chow. Data points are mean ± s.d. $N = 18$ wild-type untreated, $N = 13$ *Ndufs4*$^{-/-}$ untreated, $N = 8$ wild-type acarbose, $N = 15$ *Ndufs4*$^{-/-}$ acarbose, sex: both. **d**, Survival curves of *Ndufs4*$^{-/-}$ mice fed either control (blue) or 0.1% acarbose diet (red). Median lifespan was 56 d for control-chow-fed, and 92 d for acarbose-chow-fed mice, log-rank $P < 0.0001$. Data are pooled from two independent experiments (Extended Data Fig. 2). $N = 26$ untreated, $N = 25$ acarbose-treated, sex: both.

65% increase in median and maximum survival (Fig. 2d, pooled results, and Extended Data Fig. 2a,b, for individual cohorts). In HET3 mice, acarbose extends lifespan during normative ageing in males to a greater extent than in female animals[52,55]. However, we found no appreciable sex-specific difference in lifespan for acarbose-fed *Ndufs4*$^{-/-}$ mice (Extended Data Fig. 2c). We did not detect any sex-specific effects on weight progression in *Ndufs4*$^{-/-}$ mice, either untreated or treated with acarbose (Extended Data Fig. 2d,e). Altogether, these results indicate that acarbose successfully treats symptoms of mitochondrial disease in *Ndufs4*$^{-/-}$ mice.

Acarbose rescues *Ndufs4*$^{-/-}$ mice independently of mTOR

We investigated the putative mechanisms by which acarbose rescues disease in *Ndufs4*$^{-/-}$ mice. Acarbose is an inhibitor of alpha-glucosidases and alpha-amylases that effectively reduces absorption of carbohydrates through the intestinal mucosa[50,56,57]. Thus, we reasoned that it may act as a dietary restriction mimetic and reduce mTORC1 activity. We tested whether acarbose inhibited mTORC1 signalling in the brains of *Ndufs4*$^{-/-}$ mice by looking at the phosphorylation of ribosomal protein S6 (S6RP) via western blot. As expected, rapamycin ablated phosphorylation of S6RP in both wild-type and *Ndufs4*$^{-/-}$ animals. Conversely, mice treated with acarbose showed no appreciable reduction in S6RP phosphorylation (Extended Data Fig. 3a,b). Previous work has described hyperactivation of mTOR in brain regions from symptomatic mice during later stages of disease progression[7]; however, we did not observe this in brain samples from presymptomatic animals (p.n. day 35). We similarly observed no effect of acarbose on S6RP phosphorylation in brain samples from 50-day-old animals, though high variability among individual samples may be masking the effects of overactive mTORC1 signalling (Extended Data Fig. 4a,b).

To further assess the interaction between rapamycin and acarbose, we tested whether administering both rapamycin and acarbose would further delay the onset of neurological phenotypes and improve survival in *Ndufs4*$^{-/-}$ mice. We administered 1,000 ppm acarbose in the chow and daily intraperitoneal injections of 8 mg kg^{-1} rapamycin to *Ndufs4*$^{-/-}$ mice and control littermates beginning at weaning (p.n. day 21). To our surprise, neither control nor knockout mice tolerated the double treatment regimen. The mice were unable to gain weight (Extended Data Fig. 4c) and died within a week. To avoid this lethal effect, we reduced the frequency of rapamycin injection to every

other day, beginning at weaning. As expected, acarbose delayed the onset of clasping by 10 d. Interestingly, the effects of daily rapamycin when treatment was initiated at weaning were comparable to those of acarbose, and less than when treatment was initiated at p.n. day 10 (ref. 7). Clasping was further delayed by another 10 d in mice receiving both acarbose and every-other-day rapamycin, indicating that the two drugs have additive effects on the suppression of neurological symptoms (Extended Data Fig. 3d). Next, we determined whether double treatment with both acarbose and rapamycin could further increase survival in *Ndufs4*$^{-/-}$ mice compared with either treatment alone. Surprisingly, all three drug regimens (acarbose, daily rapamycin, acarbose and every-other-day rapamycin) had similar effects on median lifespan extension (Extended Data Fig. 3e). However, mice receiving both acarbose and every-other-day rapamycin showed a significant increase in maximum survival compared with either untreated or acarbose-treated animals. Importantly though, the double treatment did not further reduce weight and growth progression in *Ndufs4*$^{-/-}$ mice compared with rapamycin alone (Extended Data Fig. 3f,g). In parallel, we tested an alternative regimen of double treatment, beginning every-day rapamycin injections on acarbose-treated mice at p.n. day 28. Similar to every-other-day rapamycin, clasping was further delayed by this treatment regimen, compared with either treatment alone (Extended Data Fig. 4d). Similar to the every-other-day treatment, median survival was not further extended by this regimen (Extended Data Fig. 4e). Weights were comparable to *Ndufs4*$^{-/-}$ mice treated with rapamycin from weaning (Extended Data Fig. 4f,g).

Acarbose reverses metabolic dysfunction in *Ndufs4*$^{-/-}$ mice

Ndufs4$^{-/-}$ mice display prominent neurometabolic defects once neurological symptoms emerge, including accumulation of glycolytic intermediates and reduction of both fatty and amino acids in brain and liver[7]. Since acarbose significantly delays the appearance of inflammatory markers in the regions most affected by the lack of Ndufs4, we performed region-specific targeted metabolic profiling of presymptomatic (p.n. day 30) *Ndufs4*$^{-/-}$ mice fed either control or acarbose chow to determine (1) if metabolic alterations precede, and may thus be causal to, onset of disease and brain pathology; and (2) whether acarbose can prevent these alterations and generally rescue metabolic defects in these animals. We detected 138 metabolites across four different regions of the mouse brain via liquid chromatography coupled mass spectrometry (LC–MS) (Extended Data Fig. 5a). Principal component analysis (PCA) showed a clear separation by genotype in the olfactory bulb when comparing the metabolic profile of untreated wild-type and *Ndufs4*$^{-/-}$ animals, and separation by treatment when comparing untreated *Ndufs4*$^{-/-}$ animals with *Ndufs4*$^{-/-}$ animals treated with acarbose (Extended Data Fig. 6a). We applied a linear model fitting to test the group differences within each brain region. As expected from the PCA, the olfactory bulb showed the greatest number of significantly altered metabolites (47) between wild-type and *Ndufs4*$^{-/-}$ animals. Consistent with previous reports[7], *Ndufs4*$^{-/-}$ mice showed an accumulation of early glycolytic intermediates (Extended Data Fig. 5b). Treatment with acarbose significantly restored wild-type levels of most of these metabolites in the olfactory bulb (Extended Data Fig. 5c). Next, we performed metabolite set enrichment analysis and metabolite pathway analysis to determine which metabolic pathways were significantly altered in the olfactory bulb of *Ndufs4*$^{-/-}$ mice before onset of disease. Metabolite set enrichment analysis revealed that the first nine pathways differentially regulated between control and acarbose-treated *Ndufs4*$^{-/-}$ mice are all involved in carbohydrate metabolism, with glycolysis and gluconeogenesis as the most enriched (Extended Data Fig. 6b). Similarly, carbohydrate metabolic pathways were prominently featured in metabolite pathway analysis, together with glutathione metabolism and branched-chain amino acids biosynthesis (Extended Data Fig. 6c). We mapped glycolytic intermediates onto glycolysis via specific pathway analysis to better understand where the changes in glycolysis occur between untreated and treated mice (Extended Data Fig. 5d,e). Specific pathway analysis showed that early glycolytic intermediates were significantly higher in the olfactory bulb of *Ndufs4*$^{-/-}$ mice, and acarbose specifically lowered their levels to those of wild-type brains and significantly reduced pyruvate levels, further confirming that impairment in glycolysis is an early feature of disease in *Ndufs4*$^{-/-}$ mice, and suggesting that preventing this impairment may recapitulate the effects of acarbose.

We hypothesized that acarbose may relieve the overload of glycolytic intermediates by reducing glucose uptake and thus the rate of glycolysis. We compared 1-h postprandial levels of circulating glucose in wild-type and *Ndufs4*$^{-/-}$ mice treated with acarbose with those of untreated animals by measuring blood glucose concentration 1 h after the beginning of the dark cycle, when mice tend to consume their biggest meal of the day. As expected, acarbose reduced postprandial glucose in wild-type animals. However, acarbose did not further reduce blood glucose concentration in *Ndufs4*$^{-/-}$ mice, which already had lower levels than wild-type mice (Extended Data Fig. 6d). Next, we sought to determine whether direct inhibition of glycolysis could relieve symptoms of disease, similar to acarbose treatment.

To test this hypothesis, we treated *Ndufs4*$^{-/-}$ mice with two hexokinase inhibitors, 2-deoxyglucose (2-DG) and glucosamine (GlcN). These drugs are reported to reduce glycolytic flux accumulation of intermediates[58]. We monitored onset of clasping and survival. Surprisingly, neither drug increased survival nor delayed symptoms of disease in *Ndufs4*$^{-/-}$ mice (Extended Data Fig. 6e,f).

The microbiome contributes to mitochondrial disease

While conducting necropsies on *Ndufs4*$^{-/-}$ mice treated with acarbose, we noticed that their caeca and large intestines were significantly larger than those of untreated mice (Fig. 3a). Caecum enlargement is a common feature of germ-free, gnotobiotic and acarbose-fed rodents which is associated with remodelling of the intestinal flora[57,59–61]. To determine whether acarbose alters the intestinal flora of *Ndufs4*$^{-/-}$ mice, we performed 16S ribosomal DNA (rDNA) sequencing of the caecal content of *Ndufs4*$^{-/-}$ and wild-type littermates fed either a control diet or a diet supplemented with acarbose. Linear regression analysis of operational taxonomic units (OTUs) at the genus level adjusted by genotype revealed higher levels of *Bacteroides* in untreated *Ndufs4*$^{-/-}$ mice (Extended Data Fig. 7a). Acarbose significantly reduced the abundance of *Bacteroides* independently of genotype ($P = 7.3 \times 10^{-5}$, false discovery rate (FDR) = 0.001) (Fig. 3b,c and Extended Data Fig. 7a). Linear regression analysis also showed nominal significance ($P < 0.05$, FDR = 0.14) for reduction in *Prevotella* and increased abundance of *Clostridium*, *Rikenella* and *Alistipes* in the colons of acarbose-treated animals (Fig. 3b and Extended Data Fig. 7b–e). To better understand the effects of the intestinal microbiome disease aetiology and progression, we set out to deplete the endogenous intestinal microbiome in *Ndufs4*$^{-/-}$ mice by treatment with an antibiotic cocktail (ampicillin, vancomycin, metronidazole and neomycin). On average, *Ndufs4*$^{-/-}$ mice receiving the antibiotic cocktail began clasping 10 d later than untreated animals and had a median survival of 87 d (Fig. 3d,e).

Acarbose alters microbial metabolites in *Ndufs4*$^{-/-}$ mice

The effects of acarbose on murine lifespan have been linked to an increased abundance of anaerobic enteric bacteria and production of SCFAs[62]. Bacterially derived SCFAs improve nutrient metabolism and mitochondrial function in multiple organs, including the brain, by increasing mitochondrial thermogenesis and energy expenditure, providing substrates for beta-oxidation and gluconeogenesis, and modulating the activity of enzymes involved in glycolysis, TCA cycle and fatty acid catabolism in general[63,64]. We measured the concentrations of 12 SCFAs in the caecum of untreated and acarbose-treated mice via LC–MS[65] and obtained absolute concentrations for acetic, propionic, iso-butyric, butyric, 2-methyl-butyric, iso-valeric, valeric

https://doi.org/10.1038/s42255-023-00815-w

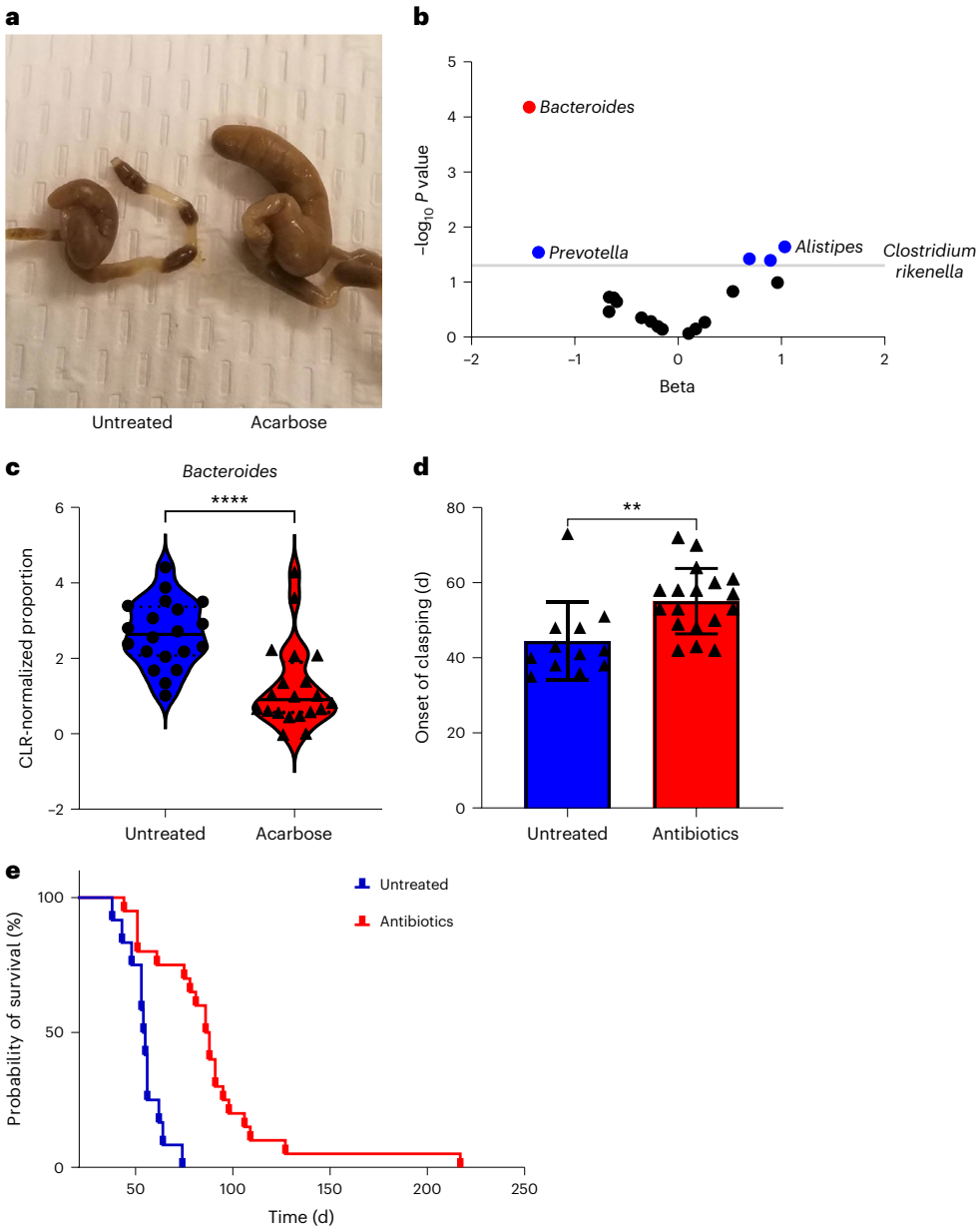

Fig. 3 | Acarbose remodels the microbiome and its metabolism in *Ndufs4*$^{-/-}$ mice. a, Representative caeca of untreated (left) and acarbose-treated (right) *Ndufs4*$^{-/-}$ mice. **b**, Volcano plot of bacterial genera in the caeca of acarbose-treated mice compared with untreated animals. Blue dots are nominally significant ($P < 0.05$, linear regression analysis) for altered abundance by acarbose treatment. Red dots are significantly altered by acarbose treatment with FDR < 0.05, linear regression analysis. Black dots indicate non-significant genera. **c**, Centred log-ratio-normalized proportion of *Bacteroides* in the caeca of untreated and acarbose-treated animals. Two-sided Student's *t*-test, $P < 0.0001$ (mean difference −1.401; 95% CI, −2.045 to −0.7572). **d**, Onset of clasping in untreated and antibiotics-treated *Ndufs4*$^{-/-}$ mice. Data are mean ± s.d. Student's *t*-test, two-sided, $P = 0.0078$ (mean difference 10.64; 95% CI, 3.122 to 18.16). $N = 12$ untreated, $N = 18$ antibiotics-treated. **e**, Survival plot of *Ndufs4*$^{-/-}$ mice treated with antibiotics cocktail (red) compared with untreated (blue). Median survival: 54.5 d untreated, 87 d antibiotics-treated. Log-rank $P < 0.0001$. $N = 12$–20. $^{**}P < 0.01$; $^{****}P < 0.0001$; CLR, centred log-ratio.

and caproic acids (Extended Data Table 1). Pairwise comparison of SCFA concentrations revealed that acarbose significantly decreased the concentrations of acetic, iso-butyric, 2-methyl-butyric, iso-valeric and valeric acid (Fig. 4a–e), while the levels of butyric acid were significantly increased (Fig. 4f). Propionic and caproic acid levels were unaffected by acarbose (Fig. 4g,h).

Microbial metabolites rescue mitochondrial disease

Since acarbose significantly alters the concentration of several SCFAs in the caecum of *Ndufs4*$^{-/-}$ mice, we hypothesized that manipulating dietary SCFAs might recapitulate some of its effect on disease progression and survival. Butyric acid was more highly represented in the caeca of both our animals and HET3 mice treated with acarbose[62]. Thus, we asked whether butyric acid supplementation could alleviate disease progression. To test this hypothesis, we treated *Ndufs4*$^{-/-}$ mice with increasing doses of tributyrin, a triacyl-glycerol ester of butyric acid. Increasing doses of tributyrin delayed onset of clasping, with 100 g kg^{-1} having effects comparable to those of acarbose (Fig. 4i). The lowest dose of tributyrin tested (10 g kg^{-1}) significantly extended median lifespan in *Ndufs4*$^{-/-}$ mice by 25%, while 50 g kg^{-1} and 100 g kg^{-1} extended survival by 13% (Fig. 4j and Extended Data Fig. 8a). Increasing doses of tributyrin also negatively affected weight gain

in *Ndufs4*$^{-/-}$ mice, as evidenced by a decreasing linear trend in both wild-type and *Ndufs4*$^{-/-}$ animals and significantly lower weights in animals treated with 100 g kg^{-1} (Fig. 4k and Extended Data Fig. 8b–d). To better understand whether butyric acid supplementation phenocopies the effects of acarbose, we treated *Ndufs4*$^{-/-}$ mice with a combination of 10 g kg^{-1} tributyrin and rapamycin, similar to the double treatment experiments with acarbose in Fig. 3. We found no significant changes in body weight (Extended Data Fig. 8e,f) and onset of clasping (Extended Data Fig. 8g) between single- and double-treated animals. However, daily administration of rapamycin to *Ndufs4*$^{-/-}$ mice on a tributyrin diet improved survival even further than tributyrin alone (Extended Data Fig. 8h, log-rank *P*: 0.0269)

Discussion

The data presented here demonstrate that acarbose is an effective treatment for mitochondrial disease in a mouse model of Leigh syndrome (Figs. 1 and 2). We tested acarbose in this context based solely on its previously documented ability to slow ageing in wild-type mice[51,52], as a test of the hypothesis that ageing and mitochondrial disease share common underlying mechanisms. To the best of our knowledge, acarbose or other alpha-glucosidase inhibitors have never been tested or proposed as a treatment for mitochondrial disease. These data are consistent with the geroscience approach to health, which posits that many, if not all, chronic age-related diseases share biological ageing as a common underlying mechanism[66,67]. Our results suggest that the geroscience approach can be successfully applied to diseases that are not obviously age-related, such as childhood mitochondrial disorders. Acarbose and rapamycin now represent two distinct examples supporting this idea, with further support provided by independent work showing that other geroprotective interventions including hypoxia[68,69], α-ketoglutarate[70] and nicotinamide mononucleotide[71] can enhance survival in the *Ndufs4*$^{-/-}$ model[72–74].

The mechanism of action for acarbose in *Ndufs4*$^{-/-}$ mice is distinct from that of rapamycin, at least at the level of mTOR inhibition. Rapamycin is a specific and potent inhibitor of mTORC1 whereas acarbose has no detectable effect on mTORC1 activity in tissues, and combination treatment with acarbose and rapamycin has partial additive effects for both neurological symptoms and survival in *Ndufs4*$^{-/-}$ mice. Interestingly, rapamycin and acarbose are each able to suppress the aberrant accumulation of glycolytic intermediates in *Ndufs4*$^{-/-}$ brain, suggesting that they may impinge on overlapping downstream mechanisms of disease rescue. Indeed, treatment with both acarbose and rapamycin increases survival in male HET3 mice beyond the historical effects of either drug alone[75], although the significance of this observation is weakened by the lack of internal controls. We unexpectedly observed synthetic lethality in very young mice treated with daily rapamycin at 8 mg kg^{-1} combined with 1,000 ppm acarbose in the chow. This lethality was not associated with loss of *Ndufs4*, as both knockout and wild-type mice were equally affected. Reducing the rapamycin treatment to every other day suppressed the effect, suggesting that the synthetic lethality results from strong mTOR inhibition combined with acarbose treatment during early development.

Metabolic imbalances arise early in some brain regions of *Ndufs4*$^{-/-}$ mice and could be causal to the disease rather than a consequence of pathology, since they are reversed by acarbose treatment before the appearance of symptoms (Extended Data Figs. 5 and 6). However, treatment with glycolytic inhibitors failed to suppress symptoms of disease in this model. Although we have not directly tested the efficacy of 2-DG and GlcN to inhibit glycolysis in *Ndufs4*$^{-/-}$ mice, the doses we tested have been well characterized and shown to reduce circulating glucose, improve insulin sensitivity and inhibit glycolysis in mice[76,77]. It is unclear whether a similar metabolic profile would arise later in life in the olfactory bulb of acarbose-treated mice, in association with the onset of neurological phenotypes, as we have not performed region-specific metabolomics on older animals. However, acarbose still reduces glial activation in the brain at p.n. day 50 (Fig. 1), which would suggest that protection from metabolic alterations may be maintained in these animals. The tissues analysed for this study were also used to analyse the effects of rapamycin on metabolite changes in specific brain regions[78]. Notably, two different methods of analysis yielded similar metabolic profiles in the olfactory bulb of untreated *Ndufs4*$^{-/-}$ mice, further strengthening the validity of our results. In accordance with approved institutional animal use protocols, mice are not allowed to reach their natural end of life; however, we do observe that acarbose-treated animals experience similar (but delayed) onset of symptoms and appear to reach the endpoint criteria in a similar manner, suggesting that they likely ultimately succumb to respiratory failure as has been previously described for *Ndufs4*$^{-/-}$ mice[6].

Although the anti-diabetic effect of acarbose is believed to arise from reduced bioavailability of simple carbohydrates resulting from intestinal alpha-glucosidase inhibition, our data strongly suggest an alternative mechanism of action involving remodelling of the gut microbiome in the *Ndufs4*$^{-/-}$ mice. We speculate that this involves dual effects of both hindering the accumulation of harmful microbial species while promoting fitness and abundance of beneficial ones. In support of this idea, we show that acarbose-treated mice have reduced abundance of *Bacteroides* and *Prevotella*, while the abundance of *Alistipes*, *Clostridium* and *Rikenella* is increased (Fig. 3). These results are consistent with observations in patients with type 2 diabetes treated with acarbose, where drug treatment consistently reduced the abundance of *Bacteroides* and efficacy of treatment correlated positively with baseline *Bacteroides* counts[79]. Our model is also consistent with the observation that complete ablation of the intestinal microbiome via treatment with antibiotics improves disease outcome in *Ndufs4*$^{-/-}$ mice (Fig. 3). Indeed, the change in *Bacteroides* observed between untreated and acarbose-treated animals is driven primarily by increased representation of this genus in *Ndufs4*$^{-/-}$ mice compared with wild-type (Extended Data Fig. 7), which suggests that loss of Complex I has direct consequences on the composition of the intestinal flora.

Fig. 4 | SCFAs recapitulate the effects of acarbose. a–**h**, Concentrations of acetic (**a**), iso-butyric (**b**), 2-methyl-butyric (**c**), iso-valeric (**d**), valeric (**e**), butyric (**f**), propionic (**g**) and caproic (**h**) acid in the caeca of untreated and acarbose-treated mice. Data are mean ± s.d. Student's *t*-test, two-sided, *P* values: acetic acid 0.0175 (mean difference −4.474; 95% CI, −8.123 to −0.8252), iso-butyric acid 0.0018 (mean difference −0.05398; 95% CI, −0.08669 to −0.02128), 2-methyl-butyric acid 0.0008 (mean difference −0.02126; 95% CI, −0.03300 to −0.009516), iso-valeric acid 0.0343 (mean difference −0.01406; 95% CI, −0.02701 to −0.001111), valeric acid <0.0001 (mean difference −0.07306; 95% CI, −0.09377 to −0.05234), butyric acid 0.0179 (mean difference 0.9046; 95% CI, 0.1642 to 1.645). *N* = 20 per group in panels **a**–**h**. **i**, Onset of clasping in *Ndufs4*$^{-/-}$ treated with increasing doses of tributyrin. Data are mean ± s.d. One-way ANOVA *P* values; untreated versus 10 g kg^{-1} tributyrin 0.0056 (mean difference −4.729; 95% CI, −8.276 to −1.182), untreated versus 100 g kg^{-1} tributyrin <0.0001 (mean difference −8.405; 95% CI, −12.41 to −4.404). *N* = 24 untreated; *N* = 15, 10 g kg^{-1} tributyrin; *N* = 8, 50 g kg^{-1} tributyrin; *N* = 11, 100 g kg^{-1} tributyrin. **j**, Survival plot of *Ndufs4*$^{-/-}$ treated with 10 g kg^{-1} tributyrin. Llog-rank *P* < 0.05. *N* = 25 untreated; *N* = 18, 10 g kg^{-1} tributyrin. **k**, Comparison of weights at 35 d p.n. for control-chow-fed wild-type, *Ndufs4*$^{-/-}$ mice and tributyrin-fed mice. One-way ANOVA adjusted *P* values: wild-type untreated versus *Ndufs4*$^{-/-}$ untreated <0.0001 (mean difference 5.543; 95% CI, 3.096 to 7.991), *Ndufs4*$^{-/-}$ untreated versus 100 g kg^{-1} tributyrin 0.0159 (mean difference 2.617; 95% CI, 0.3282 to 4.905), wild-type untreated versus wild-type 100 g kg^{-1} tributyrin 0.0022 (mean difference 3.343; 95% CI, 0.8956 to 5.791). *N* = 10 wild-type untreated, *N* = 12 *Ndufs4*$^{-/-}$ untreated, *N* = 12 wild-type 10 g kg^{-1} tributyrin, *N* = 18 *Ndufs4*$^{-/-}$ 10 g kg^{-1} tributyrin, *N* = 13 wild-type and *Ndufs4*$^{-/-}$ 50 g kg^{-1} tributyrin, *N* = 12 wild-type 100 g kg^{-1} tributyrin, *N* = 15 *Ndufs4*$^{-/-}$ 100 g kg^{-1} tributyrin. *P < 0.05; **P < 0.01; ***P < 0.001; ****P < 0.0001.

https://doi.org/10.1038/s42255-023-00815-w

Of note, the data presented here demonstrate a direct involvement of the intestinal microbiome in the aetiology and progression of a neurological mitochondrial disorder, opening an avenue to previously unforeseen mechanisms of disease and new therapeutic approaches based on the modulation of the intestinal flora and its activity. More in-depth analysis of the intestinal microbiome and its metabolic properties in *Ndufs4*$^{-/-}$ mice will provide a more detailed picture of its involvement in disease progression. These results expand on, and provide an alternative explanation for, recent observations that tetracyclines can delay disease onset in *Ndufs4*$^{-/-}$ mice by impairing mitochondrial translation[80]. Our antibiotic cocktail did not include tetracyclines, with no known beneficial effects of the other antibiotics used in the current model, emphasizing the critical role of the intestinal microbiome in mitochondrial disease.

In ageing wild-type mice, acarbose has been shown to increase the production of most SCFAs through intestinal anaerobic bacteria[62].

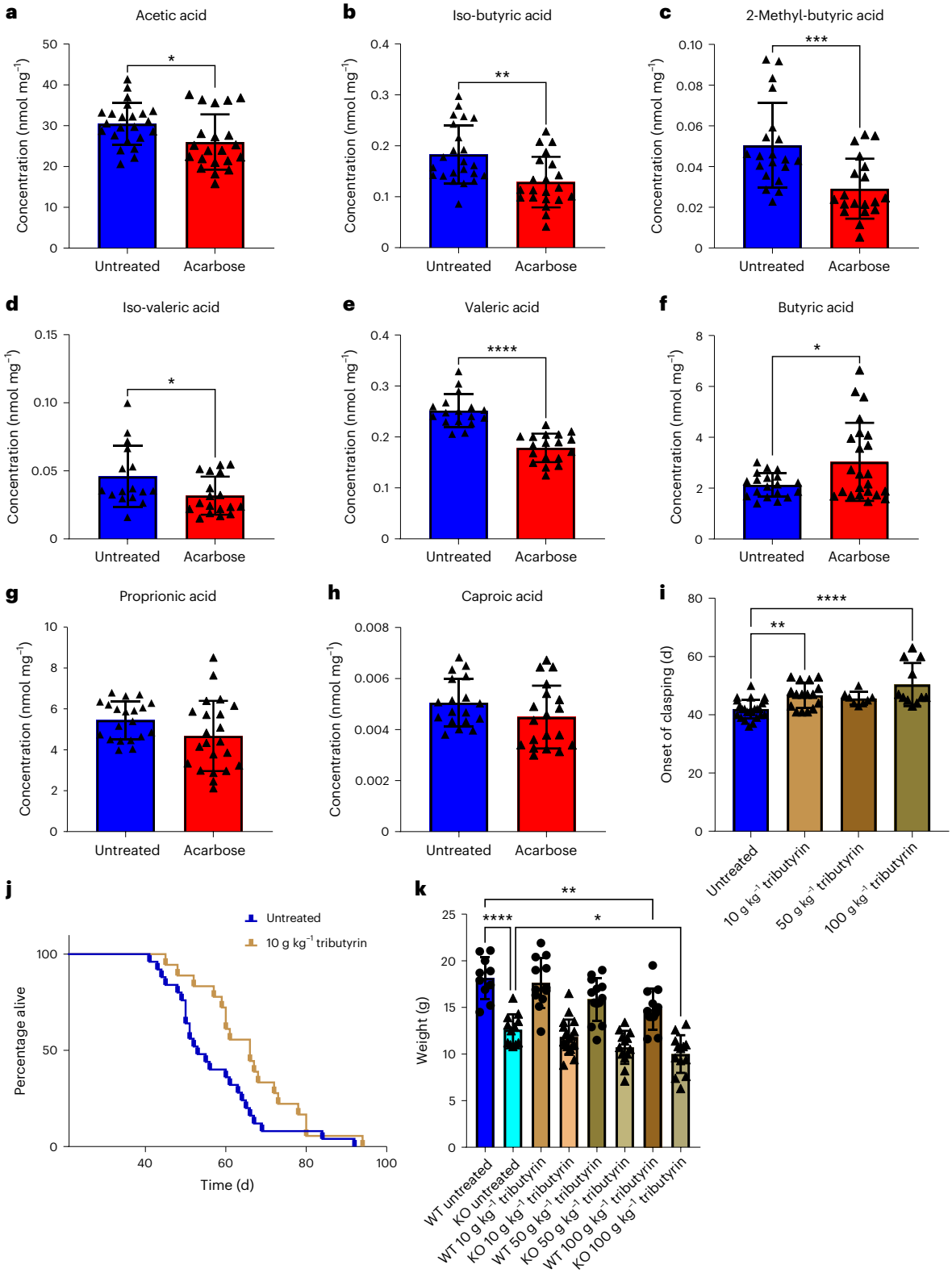

However, in our study we find that the production of some SCFAs is reduced by acarbose treatment, while production of butyric acid is increased. These differences may be ascribed to the different nature of the samples analysed (faeces versus caecal content), the strain (HET3 versus C57BL6), the vivarium location or a combination of these factors. Indeed, a more detailed and carefully controlled analysis of the metabolic activity of the intestinal microbiome in the context of both ageing and mitochondrial disease is necessary to understand the beneficial effects of acarbose in both conditions. Intriguingly, the relative abundance and metabolic activity of *Bacteroides* seem to be influenced by the luminal concentration of butyric acid, which can lower the pH of proximal areas of the large intestine, including the caecum[81]. We found that supplementation with a butyric acid source, tributyrin, was sufficient to partially phenocopy disease rescue by acarbose. While we were unable to obtain the same magnitude of effect from tributyrin as from acarbose, we note that butyrate is only one of several bioactive fermentation products altered by acarbose administration (Fig. 4). Additional strategies to modulate the levels of several SCFAs may prove more effective than perturbing the levels of only one molecule.

In conclusion, we have identified a potential avenue of treatment for Leigh syndrome and other mitochondrial diseases with acarbose, an already Food and Drug Administration-approved anti-diabetic drug that is generally considered to be safe[56]. Furthermore, we have discovered a previously overlooked connection between the intestinal flora and neurological mitochondrial disorders. These discoveries hold the potential to advance treatment of these disorders, as manipulation of the intestinal microbiome can be achieved via antibiotics, faecal matter transplants, probiotic supplementation or specific dietary regimens. While additional studies are needed to validate this hypothesis and the effectiveness of alpha-glucosidase inhibitors in other mitochondrial disorders, the current study establishes a foundation on which new approaches can be built.

Methods

Animal experiments

C57BL/6N *Ndufs4*$^{-/-}$ mice and *Ndufs4*$^{+/+}$ littermates were generated by breeding heterozygous pairs in the University of Washington Foege/Animal Research and Care Facility (ARCF) animal vivarium. All animals were genotyped before p.n. day 21, and littermate pairs of different genotypes were randomly assigned to treatments beginning around p.n. day 21. Mice that weighed less than 6.5 g at p.n. day 21 were kept in the breeder cage until they reached that weight or p.n. day 28, whichever occurred first. For 16S sequencing, wild-type and *Ndufs4*$^{-/-}$ mice from different breeder pairs were housed together to control for parental effects on microbiome composition. All animals were maintained in the Foege/ARCF animal vivarium at the University of Washington and housed in groups of two to five in either Allentown JAG 75 or Allentown NexGen Mouse 500 cages, in temperature-controlled rooms (25 °C) on racks providing filtered air and filtered, acidified water. All animals were housed on a 14-h light, 10-h dark cycle. Animals were fed Pico Lab Diet 20 5053 and treated with 1,000 ppm acarbose (Tecoland) mixed in the chow; 10 mg kg^{-1}, 50 mg kg^{-1} or 100 mg kg^{-1} tributyrin (Fisher Scientific) mixed in the chow; 1% or 10% GlcN (Fisher Scientific); 0.2% or 0.4% 2-DG (Millipore-Sigma); or daily intraperitoneal injections of 8 mg kg^{-1} rapamycin (LC Laboratories). For microbiome depletion experiments, animals were treated with a cocktail of ampicillin (1 mg ml^{-1}), vancomycin (0.5 mg ml^{-1}), metronidazole (0.5 mg ml^{-1}) and neovet (neomycin sulfate, 1 mg ml^{-1}). For survival curves and monitoring of neurological symptoms, animals were monitored two to three times a week until onset of symptoms and then monitored daily until endpoint. Animals were euthanized when they showed any of the following signs: (1) loss of over 30% of the maximum weight recorded; (2) inability to eat or drink; (3) severe lethargy, as indicated by a lack of response such as a reluctance to move when gently prodded; (4) severe respiratory difficulty while at rest, indicated by a regular pattern of deep abdominal excursions or gasping. Animals utilized for western blotting, metabolomics, 16S sequencing and SCFAs measurements were fasted overnight and re-fed for 3 h at the beginning of the following day's light cycle before cervical dislocation. Tissues were immediately snap-frozen in liquid nitrogen and stored under liquid nitrogen for further analysis. Animals utilized for histology were anaesthetised with a ketamine/xylazine mix and terminally perfused with ice-cold PBS followed by 10% neutral-buffered formalin before dissection.

Histology

Following perfusion, brains were removed from the skull and immersion-fixed in 10% neutral-buffered formalin. Coronal sections of brain at the level of the olfactory lobe, striatum and thalamus with hippocampus, and two sections of cerebellum/medulla, were obtained and routinely paraffin-embedded, sectioned at 4–5 µm and stained with haematoxylin and eosin (H&E) by the Histology and Imaging Core at the University of Washington. Immunohistochemistry for Iba1 and GFAP was performed by Harborview Medical Center Pathology Lab. Anti-GFAP (Agilent, Dako Omnis, M0761) was used at a 1:300 dilution. Anti-Iba1 (Wako Chemicals, 019-19741) was used at a 1:1,500 dilution. Slides were processed with a Leica Bond III IHC stainer, using Heat Induced Epitope retrieval with Bond Epitope Retrieval Solution 1 for 20 min and a Bond Polymer Refine detection kit (Leica Biosystems). H&E and immunohistochemistry slides were scored blindly by a board-certified veterinary pathologist (J.M.S.). For semiquantitative scoring of H&E slides, vacuolation (accompanied by neuronal loss at the higher scores) was scored on a 0–4 scale, with 0 indicating normal; 1 indicating minimal; 2 indicating mild; 3 indicating moderate; and 4 indicating severe lesions. Immunohistochemistry slides were scored semiquantitatively on a 1–4 scale, with 1 indicating expected baseline immunostaining; 2 indicating a focal cluster of more strongly immunopositive cells or multifocal or diffuse mildly increased immunopositive staining; 3 indicating moderately increased immunopositive staining (multifocal or multifocal to coalescing); and 4 indicating markedly increased coalescing to diffuse immunopositive staining. Higher-magnification images were used to evaluate microglial morphology. Representative images were taken from glass slides using an NIS-Elements BR 3.2 64-bit or captured from digital images and plated in Adobe Photoshop. For H&E images, white balance, lighting and contrast were adjusted using auto corrections applied to the entire image.

For quantitative analysis, slides were scanned in brightfield with a ×20 objective using a NanoZoomer Digital Pathology system (Hamamatsu) and digital images were then imported into Visiopharm software for analysis. Using the Visiopharm image analysis module, regions of interest were manually placed on each image, including the olfactory lobe, brainstem with vestibular nuclei and cerebellum. Visiopharm was trained to label positive staining or background tissue counterstain, and results are presented as a ratio of area of GFAP or Iba1 to total tissue area.

Western blotting

Frozen tissues were ground in liquid nitrogen, and proteins were extracted in ice-cold RIPA buffer supplemented with protease and phosphatase inhibitors. Then, 30 µg of protein extract was loaded onto NuPage Bis-Tris acrylamide gels (Thermo Fisher), and transferred onto Immobilon P membranes (Millipore-Sigma) with a BioRad Trans-Blot Turbo Transfer System (BioRad). Membranes were blotted with antibodies against phospho-S6 (Ser 235–236, cat. no. 2211), total S6 (clone 5G10) and TREM2 (clone D8I4C) (Cell Signaling).

Metabolomics

The olfactory bulb, brainstem and cerebellum were dissected from freshly isolated brains and snap-frozen for further analysis. All samples

were submitted to the Northwest Metabolomics Research Center at the University of Washington.

Brain samples were thawed at 4 °C and homogenized in 200 µl of PBS. Then, 800 µl of methanol containing 53.1 µM ^{13}C-arginine and 50.1 µM ^{13}C-glucose (Sigma-Aldrich) was added, and the samples were incubated for 30 min at −70 °C. The suspension was sonicated in an ice bath for 10 min and then centrifuged at 20,800*g* for 10 min at 0–4 °C. Supernatants (600 µl) were collected and dried for 60 min using an Eppendorf Vacufuge Drier; then each was reconstituted in 600 µl of 40% Solution A and 60% Solution B, also containing 5.13 µM ^{13}C-tyrosine and 22.6 µM ^{13}C-lactate. Solution A was 30 mM ammonium acetate in 85% H_2O/15% acetonitrile and 0.2% acetic acid. Solution B was 15% H_2O/85% acetonitrile and 0.2% acetic acid. Reagents for these solutions were purchased from Fisher Scientific. All samples were then filtered through Millipore PVDF filters immediately before chromatography.

The liquid chromatography system was composed of two Agilent 1260 binary pumps, an Agilent 1260 auto-sampler and an Agilent 1290 column compartment containing a column-switching valve (Agilent). Each sample was injected twice, 10 µl for analysis using negative ionization mode and 2 µl for analysis using positive ionization mode. Both chromatographic separations were performed in hydrophilic interaction chromatography mode on two parallel Waters XBridge BEH Amide columns (150 × 2.1 mm^2, 2.5-µm particle size, Waters). While one column was performing the separation, the other column was reconditioned and ready for the next injection. The flow rate was 0.300 ml min^{-1}, the auto-sampler temperature was kept at 4 °C and the column compartment was set at 40 °C, and total separation time for both ionization modes was 20 min. The gradient conditions for both separations were identical and consisted of 10% Solvent A from 0 to 2 min, a ramp to 50% during minutes 2–5, continued 50% Solvent A from 5 to 9 min, a ramp back to 10% from 9 to 11 min and then 10% Solvent A from 11 to 20 min.

After the chromatographic separation, mass spectrometry ionization and data acquisition were performed using an AB Sciex QTrap 5500 mass spectrometer (AB Sciex) equipped with an electrospray ionization source. The instrument was controlled by Analyst 1.5 software (AB Sciex). Targeted data acquisition was performed in Multiple Reaction Monitoring (MRM) mode. The source and collision gas was N_2 (99.999% purity). The ion source conditions in negative mode were as follows: Curtain Gas (CUR) = 25 psi, Collision Gas (CAD) = high, Ion Spray Voltage (IS) = −3.8 kV, Temperature (TEM) = 500 °C, Ion Source Gas 1 (GS1) = 50 psi and Ion Source Gas 2 (GS2) = 40 psi. The ion source conditions in positive mode were as follows: CUR = 25 psi, CAD = high, IS = 3.8 kV, TEM = 500 °C, GS1 = 50 psi and GS2 = 40 psi.

Blood glucose measurements

Blood glucose was measured 1 h after the beginning of the dark cycle with an Alpha Trak 2 glucometer at day 35 p.n. (Zoetis).

16S rDNA sequencing

Caecum content was collected at the time of necropsy and snap-frozen in liquid nitrogen. Samples were submitted to RTL Genomics (Lubbock, TX) for sequencing and identification. rDNA extracts were sequenced on Illumina MySeq sequencers. Raw sequences were denoised using the following steps: (1) Forward and reverse reads in FASTQ format were merged together using the PEAR Illumina paired-end read merger. (2) Paired FASTQ files were then converted into FASTA formatted sequences and trimmed back at the last base with a total average read greater than 25. (3) Sequences were sorted by length and run through the USEARCH algorithm to perform prefix dereplication and clustering at 4% divergence. (4) OTUs were selected with the UPARSE OTU algorithm and chimera checking was performed on the selected OTUs with the UCHIME detection software in de novo mode. (5) Clusters were then mapped to their corresponding OTUs, chimeric sequences removed and individual reads mapped to the clusters. OTU taxonomic assignments were determined by USEARCH alignments against a database of high-quality sequences derived from the NCBI database.

SCFA analysis

First, 50–100 mg of cryoground caecum content was weighed into Precellys Soft Tissue Homogenizing CK14 tubes (Bertin) and shipped to the Duke Proteomics and Metabolomics Core at Duke University for analysis. Caecum samples were extracted and derivatized by 3-nitrophenylhydrazine (3-NPH) as previously described[65]. Briefly, 50:50 ethanol/water was added at a ratio of 10 µl per 1 mg. All tubes were homogenized on the Precellys 24 bead blaster (Bertin) at 10 °C for three cycles at 10,000 r.p.m. Then, 20 µl from each sample was derivatized by adding 20 µl of 200 mM 3-NPH in 50% ethanol with 6% pyridine and 120 mM *N*-(3-dimethylaminopropyl)-*N*′-ethylcarbodiimide hydrochloride (EDC·HCl) in 50% ethanol, and incubating at 35 °C for 30 min while shaking. The reaction was quenched with 760 µl of cold 10% ethanol in water with 1% formic acid and held at 4 °C. Data collection was performed using LC–MS/MS on a Sciex 6500+ QTRAP mass spectrometer (Sciex), including calibration curves for each analyte and a ^{13}C6 internal standard for each compound (via ^{13}C6 NPH derivatization reagent).

Ultra-high pressure liquid chromatography separation of the SCFAs was performed using an Exion AD liquid chromatograph (Sciex) with a Waters Acquity 2.1 × 50 mm^2 1.7-µm BEH C18 column fitted with a Waters Acquity C18 1.7-µm VanGuard column. Analytes were separated using a gradient from 15% solvent B to 100% solvent B in 9.5 min. Solvents A and B were 0.1% formic acid in water and acetonitrile, respectively. The total UPLC analysis time was approximately 13.5 min. The method uses electrospray ionization in negative mode introduced into a 6500+ QTrap mass spectrometer (Sciex) operating in the MRM mode. MRM transitions (compound-specific precursor to product ion transitions) for each analyte and internal standard were collected over the appropriate retention time window. The standard curve was run once at the beginning of the run queue and once at the end of the sample run queue. The Golden West Quality Controls (QCs), study pool QC (SPQC) and calibration QCs were run once at the beginning, once in the middle and once at the end of the run queue. Injection volume for each injection was 5 µl.

All data were analysed in Skyline v.21.1.1 (www.skyline.ms)[82], which includes raw data import, peak integration and a linear regression fit with 1/×2 weighting for the calibration curves.

The calibration curves for all of the analytes contain 12 points, from 0.98 µM to 10 mM for acetic acid, and from 0.098 to 1 mM for the other analytes. Each calibrator's residual bias was calculated after regression fit, and any points other than the lower and upper limits of quantitation where the residual fell outside of 15% were removed from the calibration curve equation. The lower limit of quantitation (LLOQ) was defined as the lowest point that met the criterion of having a bias <20%, and the upper limit of quantitation (ULOQ) was defined in the same way for the highest point. The calibration range used for concentration calculations in the samples is listed in Extended Data Table 1 for each analyte.

Statistical analysis

Unless otherwise stated, all data were analysed using the GraphPad Prism 9 software. *P* values of 0.05 or lower were considered statistically significant.

Statistical analysis for metabolomics data was carried out using R (v.4.0.2). The targeted metabolomics assay was designed to detect 210 metabolites, and 138 of these metabolites were detected in at least one sample. We performed a median normalization where we adjusted the data, so all samples have the same median value of the metabolite abundance post $\log_2$ transformation. Then, 135 metabolites with <20% missingness and a coefficient of variation < 20% in the pooled sample QC data were included in further analysis. After filtering, no missing values remained, and therefore, no imputation was performed.

PCA was performed on the transformed and normalized dataset using R prcomp() function. We fit linear models to the normalized and filtered data using the Bioconductor limma package[83] to assess the difference in abundance between the groups within each brain region while adjusting for the sample collection month in the model. The limma package uses empirical Bayes moderated statistics, which improves power by 'borrowing strength' between metabolites to moderate the residual variance[84]. We selected metabolites with an FDR of 10%, and pathway analyses were conducted with MetaboAnalyst 5.0 (ref. 85).

16S sequence taxonomic regression analysis

The proportional 16S read abundances of each sample's genus-level taxa were centred and log-ratio transformed using the clr() function of the 'compositions' R package (https://cran.r-project.org/web/packages/compositions/index.html). Linear regression models using the base R lm() function were used to determine the acarbose exposure treatment association with the clr transformed taxa outcome while adjusting for sex and cage segregation. Common taxa with a mean proportional abundance >0.01 were tested. FDR adjustments to *P* values were made using the R p.adjust() function with the Benjamini and Hochberg method[86]. Nominal significance was set at $P < 0.05$, and statistically significant taxa are reported with an FDR < 0.05.

Ethics statement

All animal experiments were reviewed and approved by the University of Washington Institutional Animal Care and Use Committee.

Reporting summary

Further information on research design is available in the Nature Portfolio Reporting Summary linked to this article.

Data availability

The data used to generate the figures in this manuscript are publicly available and published along with the paper. Further information and requests for resources and reagents should be directed to and will be fulfilled by Alessandro Bitto (ab62@uw.edu). Source data are provided with this paper.

References

1. Janssen, R. J., Nijtmans, L. G., van den Heuvel, L. P. & Smeitink, J. A. Mitochondrial complex I: structure, function and pathology. *J. Inherit. Metab. Dis.* **29**, 499–515 (2006).
2. Wallace, D. C. Mitochondrial DNA mutations in disease and aging. *Environ. Mol. Mutagen.* **51**, 440–450 (2010).
3. Bannwarth, S. et al. Prevalence of rare mitochondrial DNA mutations in mitochondrial disorders. *J. Med. Genet.* **50**, 704–714 (2013).
4. Fassone, E. & Rahman, S. Complex I deficiency: clinical features, biochemistry and molecular genetics. *J. Med. Genet.* **49**, 578–590 (2012).
5. Budde, S. M. et al. Combined enzymatic complex I and III deficiency associated with mutations in the nuclear encoded NDUFS4 gene. *Biochem. Biophys. Res. Commun.* **275**, 63–68 (2000).
6. Kruse, S. E. et al. Mice with mitochondrial complex I deficiency develop a fatal encephalomyopathy. *Cell Metab.* **7**, 312–320 (2008).
7. Johnson, S. C. et al. mTOR inhibition alleviates mitochondrial disease in a mouse model of Leigh syndrome. *Science* **342**, 1524–1528 (2013).
8. Johnson, S. C. et al. Dose-dependent effects of mTOR inhibition on weight and mitochondrial disease in mice. *Front. Genet.* **6**, 247 (2015).
9. Kim, S. H. et al. Multi-organ abnormalities and mTORC1 activation in zebrafish model of multiple acyl-CoA dehydrogenase deficiency. *PLoS Genet.* **9**, e1003563 (2013).
10. Peng, M. et al. Inhibiting cytosolic translation and autophagy improves health in mitochondrial disease. *Hum. Mol. Genet.* **24**, 4829–4847 (2015).
11. Ito, T. K. et al. Hepatic S6K1 partially regulates lifespan of mice with mitochondrial complex I deficiency. *Front. Genet.* **8**, 113 (2017).
12. Martin-Perez, M. et al. PKC downregulation upon rapamycin treatment attenuates mitochondrial disease. *Nat. Metab.* **2**, 1472–1481 (2020).
13. Johnson, S. C. et al. mTOR inhibitors may benefit kidney transplant recipients with mitochondrial diseases. *Kidney Int.* **95**, 455–466 (2019).
14. Sage-Schwaede, A. et al. Exploring mTOR inhibition as treatment for mitochondrial disease. *Ann. Clin. Transl. Neurol.* **6**, 1877–1881 (2019).
15. Powers, R. W. 3rd, Kaeberlein, M., Caldwell, S. D., Kennedy, B. K. & Fields, S. Extension of chronological life span in yeast by decreased TOR pathway signaling. *Genes Dev.* **20**, 174–184 (2006).
16. Robida-Stubbs, S. et al. TOR signaling and rapamycin influence longevity by regulating SKN-1/Nrf and DAF-16/FoxO. *Cell Metab.* **15**, 713–724 (2012).
17. Bjedov, I. et al. Mechanisms of life span extension by rapamycin in the fruit fly *Drosophila melanogaster*. *Cell Metab.* **11**, 35–46 (2010).
18. Harrison, D. E. et al. Rapamycin fed late in life extends lifespan in genetically heterogeneous mice. *Nature* **460**, 392–395 (2009).
19. Anisimov, V. N. et al. Rapamycin increases lifespan and inhibits spontaneous tumorigenesis in inbred female mice. *Cell Cycle* **10**, 4230–4236 (2011).
20. Komarova, E. A. et al. Rapamycin extends lifespan and delays tumorigenesis in heterozygous $p53^{+/-}$ mice. *Aging (Albany NY)* **4**, 709–714 (2012).
21. Wilkinson, J. E. et al. Rapamycin slows aging in mice. *Aging Cell* **11**, 675–682 (2012).
22. Livi, C. B. et al. Rapamycin extends life span of $Rb1^{+/-}$ mice by inhibiting neuroendocrine tumors. *Aging (Albany NY)* **5**, 100–110 (2013).
23. Neff, F. et al. Rapamycin extends murine lifespan but has limited effects on aging. *J. Clin. Investig.* **123**, 3272–3291 (2013).
24. Fok, W. C. et al. Mice fed rapamycin have an increase in lifespan associated with major changes in the liver transcriptome. *PLoS ONE* **9**, e83988 (2014).
25. Miller, R. A. et al. Rapamycin-mediated lifespan increase in mice is dose and sex dependent and metabolically distinct from dietary restriction. *Aging Cell* **13**, 468–477 (2014).
26. Popovich, I. G. et al. Lifespan extension and cancer prevention in HER-2/neu transgenic mice treated with low intermittent doses of rapamycin. *Cancer Biol. Ther.* **15**, 586–592 (2014).
27. Bitto, A. et al. Transient rapamycin treatment can increase lifespan and healthspan in middle-aged mice. *eLife* **5**, e16351 (2016).
28. Miller, R. A. et al. Rapamycin, but not resveratrol or simvastatin, extends life span of genetically heterogeneous mice. *J. Gerontol. A Biol. Sci. Med. Sci.* **66**, 191–201 (2011).
29. Zhang, Y. et al. Rapamycin extends life and health in C57BL/6 mice. *J. Gerontol. A Biol. Sci. Med. Sci.* **69**, 119–130 (2014).
30. Halloran, J. et al. Chronic inhibition of mammalian target of rapamycin by rapamycin modulates cognitive and non-cognitive components of behavior throughout lifespan in mice. *Neuroscience* **223**, 102–113 (2012).
31. Majumder, S. et al. Lifelong rapamycin administration ameliorates age-dependent cognitive deficits by reducing IL-1β and enhancing NMDA signaling. *Aging Cell* **11**, 326–335 (2012).
32. Zaseck, L. W., Miller, R. A. & Brooks, S. V. Rapamycin attenuates age-associated changes in tibialis anterior tendon viscoelastic properties. *J. Gerontol. A Biol. Sci. Med. Sci.* **71**, 858–865 (2016).

33. Chiao, Y. A. et al. Rapamycin transiently induces mitochondrial remodeling to reprogram energy metabolism in old hearts. *Aging (Albany NY)* **8**, 314–327 (2016).
34. Dai, D. F. et al. Altered proteome turnover and remodeling by short-term caloric restriction or rapamycin rejuvenate the aging heart. *Aging Cell* **13**, 529–539 (2014).
35. Flynn, J. M. et al. Late-life rapamycin treatment reverses age-related heart dysfunction. *Aging Cell* **12**, 851–862 (2013).
36. Chen, C., Liu, Y. & Zheng, P. mTOR regulation and therapeutic rejuvenation of aging hematopoietic stem cells. *Sci. Signal.* **2**, ra75 (2009).
37. Shavlakadze, T. et al. Short-term low-dose mTORC1 inhibition in aged rats counter-regulates age-related gene changes and blocks age-related kidney pathology. *J. Gerontol. A Biol. Sci. Med. Sci.* **73**, 845–852 (2018).
38. An, J. Y. et al. Rapamycin rejuvenates oral health in aging mice. *eLife* **9**, e54318 (2020).
39. An, J. Y. et al. Rapamycin treatment attenuates age-associated periodontitis in mice. *Geroscience* **39**, 457–463 (2017).
40. Yilmaz, O. H. et al. mTORC1 in the Paneth cell niche couples intestinal stem-cell function to calorie intake. *Nature* **486**, 490–495 (2012).
41. Garcia, D. N. et al. Effect of caloric restriction and rapamycin on ovarian aging in mice. *Geroscience* **41**, 395–408 (2019).
42. Urfer, S. R. et al. A randomized controlled trial to establish effects of short-term rapamycin treatment in 24 middle-aged companion dogs. *Geroscience* **39**, 117–127 (2017).
43. Mannick, J. B. et al. mTOR inhibition improves immune function in the elderly. *Sci. Transl. Med.* **6**, 268ra179 (2014).
44. Mannick, J. B. et al. TORC1 inhibition enhances immune function and reduces infections in the elderly. *Sci. Transl. Med.* **10**, eaaq1564 (2018).
45. Lopez-Otin, C., Blasco, M. A., Partridge, L., Serrano, M. & Kroemer, G. The hallmarks of aging. *Cell* **153**, 1194–1217 (2013).
46. Srivastava, S. The mitochondrial basis of aging and age-related disorders. *Genes (Basel)* **8**, 398 (2017).
47. Trifunovic, A. & Larsson, N. G. Mitochondrial dysfunction as a cause of ageing. *J. Intern. Med.* **263**, 167–178 (2008).
48. Berry, B. J. & Kaeberlein, M. An energetics perspective on geroscience: mitochondrial protonmotive force and aging. *Geroscience* **43**, 1591–1604 (2021).
49. Bitto, A. Is aging an acquired mitochondrial disease? *Innov. Aging* **3**, S394–S395 (2019).
50. Hoffmann, J. & Spengler, M. Efficacy of 24-week monotherapy with acarbose, metformin, or placebo in dietary-treated NIDDM patients: the Essen-II Study. *Am. J. Med.* **103**, 483–490 (1997).
51. Harrison, D. E. et al. Acarbose improves health and lifespan in aging HET3 mice. *Aging Cell* **18**, e12898 (2019).
52. Strong, R. et al. Longer lifespan in male mice treated with a weakly estrogenic agonist, an antioxidant, an α-glucosidase inhibitor or a Nrf2-inducer. *Aging Cell* **15**, 872–884 (2016).
53. Quintana, A., Kruse, S. E., Kapur, R. P., Sanz, E. & Palmiter, R. D. Complex I deficiency due to loss of Ndufs4 in the brain results in progressive encephalopathy resembling Leigh syndrome. *Proc. Natl Acad. Sci. USA* **107**, 10996–11001 (2010).
54. Kayser, E. B., Sedensky, M. M. & Morgan, P. G. Region-specific defects of respiratory capacities in the Ndufs4(KO) mouse brain. *PLoS ONE* **11**, e0148219 (2016).
55. Harrison, D. E. et al. Acarbose, 17-α-estradiol, and nordihydroguaiaretic acid extend mouse lifespan preferentially in males. *Aging Cell* **13**, 273–282 (2014).
56. DiNicolantonio, J. J., Bhutani, J. & O'Keefe, J. H. Acarbose: safe and effective for lowering postprandial hyperglycaemia and improving cardiovascular outcomes. *Open Heart* **2**, e000327 (2015).
57. Lembcke, B., Loser, C., Folsch, U. R., Wohler, J. & Creutzfeldt, W. Adaptive responses to pharmacological inhibition of small intestinal α-glucosidases in the rat. *Gut* **28**, 181–187 (1987).
58. Wick, A. N., Drury, D. R., Nakada, H. I. & Wolfe, J. B. Localization of the primary metabolic block produced by 2-deoxyglucose. *J. Biol. Chem.* **224** 963–969 (1957).
59. Gordon, H. A. & Pesti, L. The gnotobiotic animal as a tool in the study of host microbial relationships. *Bacteriol. Rev.* **35**, 390–429 (1971).
60. Reikvam, D. H. et al. Depletion of murine intestinal microbiota: effects on gut mucosa and epithelial gene expression. *PLoS ONE* **6**, e17996 (2011).
61. Savage, D. C. & Dubos, R. Alterations in the mouse cecum and its flora produced by antibacterial drugs. *J. Exp. Med.* **128**, 97–110 (1968).
62. Smith, B. J. et al. Changes in the gut microbiome and fermentation products concurrent with enhanced longevity in acarbose-treated mice. *BMC Microbiol.* **19**, 130 (2019).
63. Koh, A., De Vadder, F., Kovatcheva-Datchary, P. & Backhed, F. From dietary fiber to host physiology: short-chain fatty acids as key bacterial metabolites. *Cell* **165**, 1332–1345 (2016).
64. Bourassa, M. W., Alim, I., Bultman, S. J. & Ratan, R. R. Butyrate, neuroepigenetics and the gut microbiome: can a high fiber diet improve brain health? *Neurosci. Lett.* **625**, 56–63 (2016).
65. Han, J., Lin, K., Sequeira, C. & Borchers, C. H. An isotope-labeled chemical derivatization method for the quantitation of short-chain fatty acids in human feces by liquid chromatography-tandem mass spectrometry. *Anal. Chim. Acta* **854**, 86–94 (2015).
66. Kennedy, B. K. et al. Geroscience: linking aging to chronic disease. *Cell* **159**, 709–713 (2014).
67. Kaeberlein, M. Translational geroscience: a new paradigm for 21st century medicine. *Transl. Med. Aging* **1**, 1–4 (2017).
68. Leiser, S. F., Fletcher, M., Begun, A. & Kaeberlein, M. Life-span extension from hypoxia in *Caenorhabditis elegans* requires both HIF-1 and DAF-16 and is antagonized by SKN-1. *J. Gerontol. A Biol. Sci. Med. Sci.* **68**, 1135–1144 (2013).
69. Mehta, R., Chandler-Brown, D., Ramos, F. J., Shamieh, L. S. & Kaeberlein, M. Regulation of mRNA translation as a conserved mechanism of longevity control. *Adv. Exp. Med. Biol.* **694**, 14–29 (2010).
70. Asadi Shahmirzadi, A. et al.Alpha-ketoglutarate, an endogenous metabolite, extends lifespan and compresses morbidity in aging mice.*Cell Metab.* **32**, 447–456.e6 (2020).
71. Mills, K. F. et al. Long-term administration of nicotinamide mononucleotide mitigates age-associated physiological decline in mice. *Cell Metab.* **24**, 795–806 (2016).
72. Jain, I. H. et al. Hypoxia as a therapy for mitochondrial disease. *Science* **352**, 54–61 (2016).
73. Ferrari, M. et al. Hypoxia treatment reverses neurodegenerative disease in a mouse model of Leigh syndrome. *Proc. Natl Acad. Sci. USA* **114**, E4241–E4250 (2017).
74. Lee, C. F., Caudal, A., Abell, L., Nagana Gowda, G. A. & Tian, R. Targeting NAD^+ metabolism as interventions for mitochondrial disease. *Sci. Rep.* **9**, 3073 (2019).
75. Strong, R. et al. Lifespan benefits for the combination of rapamycin plus acarbose and for captopril in genetically heterogeneous mice. *Aging Cell* **21**, e13724 (2022).
76. Weimer, S. et al. D-Glucosamine supplementation extends life span of nematodes and of ageing mice. *Nat. Commun.* **5**, 3563 (2014).
77. Singh, S. et al. Chronic dietary administration of the glycolytic inhibitor 2-deoxy-D-glucose (2-DG) inhibits the growth of implanted Ehrlich's ascites tumor in mice. *PLoS ONE* **10**, e0132089 (2015).

78. Johnson, S. C. et al. Regional metabolic signatures in the Ndufs4(KO) mouse brain implicate defective glutamate/α-ketoglutarate metabolism in mitochondrial disease. *Mol. Genet. Metab.* **130**, 118–132 (2020).
79. Gu, Y. et al. Analyses of gut microbiota and plasma bile acids enable stratification of patients for antidiabetic treatment. *Nat. Commun.* **8**, 1785 (2017).
80. Perry, E. A. et al. Tetracyclines promote survival and fitness in mitochondrial disease models. *Nat. Metab.* **3**, 33–42 (2021).
81. Rios-Covian, D., Salazar, N., Gueimonde, M. & de Los Reyes-Gavilan, C. G. Shaping the metabolism of intestinal *Bacteroides* population through diet to improve human health. *Front. Microbiol.* **8**, 376 (2017).
82. MacLean, B. et al. Skyline: an open source document editor for creating and analyzing targeted proteomics experiments. *Bioinformatics* **26**, 966–968 (2010).
83. Ritchie, M. E. et al. limma powers differential expression analyses for RNA-sequencing and microarray studies. *Nucleic Acids Res.* **43**, e47 (2015).
84. Smyth, G. K. Linear models and empirical Bayes methods for assessing differential expression in microarray experiments. *Stat. Appl. Genet. Mol. Biol.* **3**, Article3 (2004).
85. Pang, Z. et al. MetaboAnalyst 5.0: narrowing the gap between raw spectra and functional insights. *Nucleic Acids Res.* **49**, W388–W396 (2021).
86. Benjamini, Y. & Hochberg, Y. Controlling the false discovery rate: a practical and powerful approach to multiple testing. *J. R. Stat. Soc. Series B Stat. Methodol.* **57**, 289–300 (1995).

Acknowledgements

We acknowledge funding from the Nathan Shock Center of Excellence for the Biology of Aging (grant no. 3 P30 AG 013280) and from grant no. 1 R01 NS98329 Mechanisms of Mitochondrial Disease Suppression in Ndufs4 Knockout Mice.

Author contributions

A.B. and M.K. devised the study. A.B., A.S.G., B.M.G.N., H.T., K.S., N.T.,G.V., J.B. and A.S. administered treatments, collected weight data and scored neurological phenotypes and survival. A.B., H.T., K.S., A.S. and N.T. collected tissues and ran western blot analyses. A.B., A.S.G., B.M.G.N., H.T., K.S., N.T., G.V. and S.R.U. helped maintain the mouse colony and genotyped animals. I.B.S. and W.D. helped with the design, execution and analysis of microbiome sequencing data. K.Y. and L.W. helped with the analysis of metabolomics data. E.-B.K. helped with the design and collection of samples for metabolomics analysis. J.M.S. performed all histopathology scoring. D.L.S. Jr. contributed acarbose and scientific rationale for the study. J.W.T. and L.D. measured the abundance of SCFAs. T.K.I. measured survival and neurological symptoms onset in mice treated with antibiotics. A.B. and M.K. wrote the manuscript.

Competing interests

The authors declare no competing interests.

Additional information

Extended data is available for this paper at https://doi.org/10.1038/s42255-023-00815-w.

Supplementary information The online version contains supplementary material available at https://doi.org/10.1038/s42255-023-00815-w.

Correspondence and requests for materials should be addressed to Matt Kaeberlein.

Peer review information *Nature Metabolism* thanks Albert Quintana and the other, anonymous, reviewer(s) for their contribution to the peer review of this work. Primary Handling Editor: Christoph Schmitt, in collaboration with the *Nature Metabolism* team.

Reprints and permissions information is available at www.nature.com/reprints.

Publisher's note Springer Nature remains neutral with regard to jurisdictional claims in published maps and institutional affiliations.

Alessandro Bitto[1], Anthony S. Grillo[1], Takashi K. Ito[1,14], Ian B. Stanaway[2,3], Bao M. G. Nguyen[1], Kejun Ying[4], Herman Tung[5], Kaleb Smith[6], Ngoc Tran[1], Gunnar Velikanje[1], Silvan R. Urfer[1], Jessica M. Snyder[7], Jacob Barton[1], Ayush Sharma[1], Ernst-Bernhard Kayser[8], Lu Wang[9], Daniel L. Smith Jr.[10], J. Will Thompson[11], Laura DuBois[12], William DePaolo[13] & Matt Kaeberlein[1]

[1]Department of Laboratory Medicine and Pathology, University of Washington, Seattle, WA, USA. [2]Division of Nephrology, School of Medicine, University of Washington, Seattle, WA, USA. [3]Harborview Medical Center, Kidney Research Institute, Seattle, WA, USA. [4]T.H. Chan School of Public Health, Harvard University, Boston, MA, USA. [5]Shape Therapeutics, Seattle, WA, USA. [6]Seattle Genetics, Seattle, WA, USA. [7]Department of Comparative Medicine, University of Washington, Seattle, WA, USA. [8]Seattle Children's Research Institute, Seattle, WA, USA. [9]Department of Environmental and Occupational Health Sciences, University of Washington, Seattle, WA, USA. [10]Department of Nutrition Sciences, University of Alabama at Birmingham, Birmingham, AL, USA. [11]Department of Pharmacology and Cancer Biology, Duke University, Durham, NC, USA. [12]Department of Biostatistics and Bioinformatics, Duke University, Durham, NC, USA. [13]Department of Microbiology, University of Washington, Seattle, WA, USA. [14]Present address: RIKEN Center for Sustainable Resource Science, Saitama, Japan. ✉e-mail: kaeber@uw.edu

https://doi.org/10.1038/s42255-023-00815-w

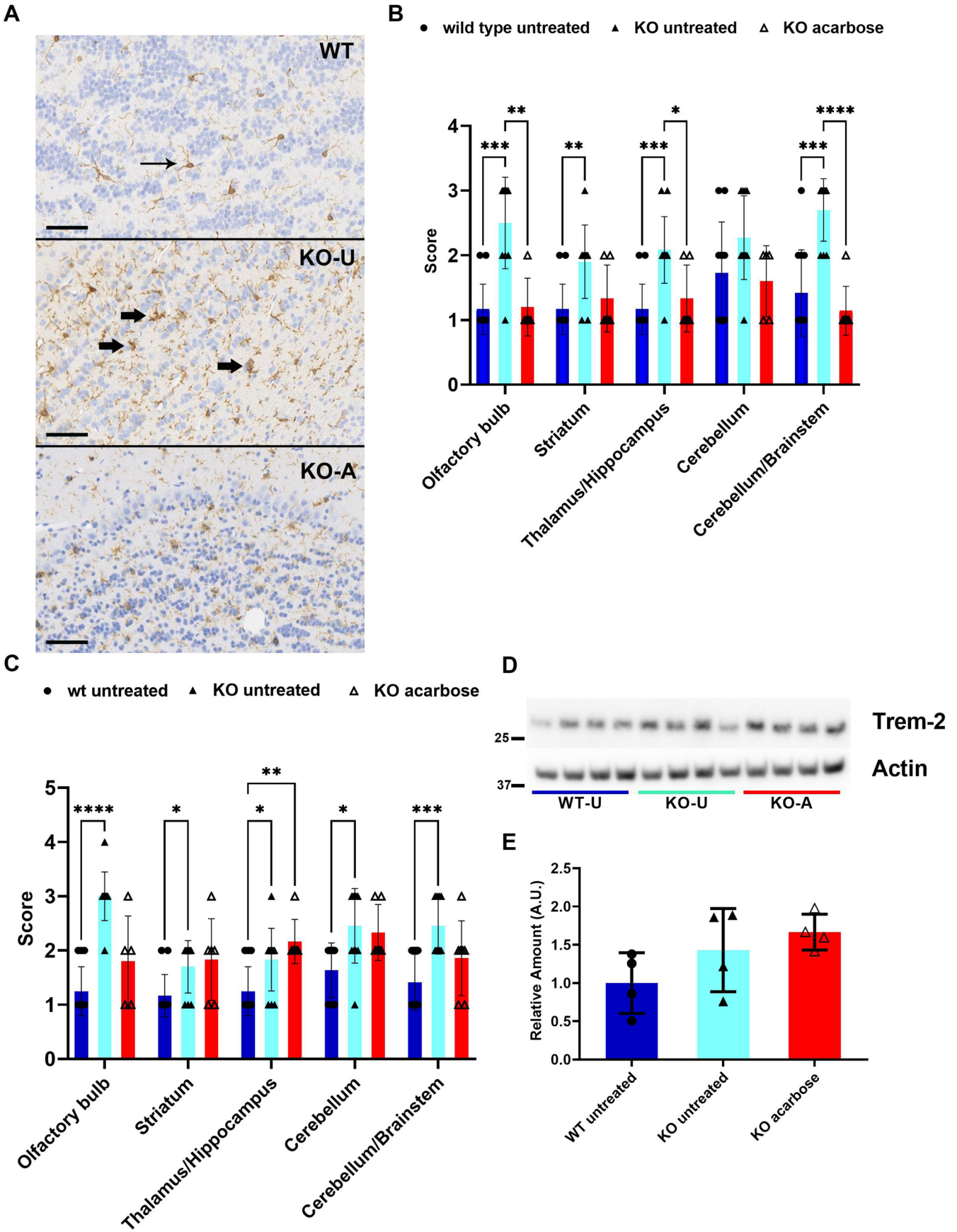

Extended Data Fig. 1 | See next page for caption.

https://doi.org/10.1038/s42255-023-00815-w

Extended Data Fig. 1 | Acarbose reduces brain inflammation in *Ndufs4*$^{-/-}$ mice. (**a**) Semi-quantitative immunohistochemistry for GFAP (**b**) and Iba1 (**c**) in several brain regions. Data are presented as individual values (closed circles wild type untreated, closed triangles *Ndufs4*$^{-/-}$ untreated, open triangles *Ndufs4*$^{-/-}$ acarbose-treated), superimposed on mean +/− standard deviation. Mixed-Effect Model p-values; GFAP; wild type untreated vs *Ndufs4*$^{-/-}$ untreated =0.0003 (mean difference −1.333, 95% CI −1.992 to −0.6751), Striatum =0.0088 (mean difference = −0.7333, 95% CI −1.282 to −0.1851), Thalamus/Hippocampus =0.0002 (mean difference = −0.9167, 95% CI −1.387 to −0.4461), Cerebellum/Brainstem =0.0001 (mean difference −1.283, 95% CI −1.907 to −0.6598), *Ndufs4*$^{-/-}$ untreated vs. *Ndufs4*$^{-/-}$ acarbose-treated, olfactory bulb = 0.0026 (mean difference =1.3, 95% CI interval 0.4992 to 2.101), Thalamus/Hippocampus =0.0378 (mean difference =0.75, 95% CI 0.04374 to 1.456), cerebellum/brainstem, <0.0001 (mean difference =1.557, 95% CI 1.013 to 2.101); Iba1; wild type untreated vs *Ndufs4*$^{-/-}$ untreated, olfactory bulb <0.0001 (mean difference −1.75, −2.223 to −1.277), striatum =0.0303 (mean difference −0.5333, 95% CI −1.019 to −0.0475), Thalamus/Hippocampus =0.0307 (mean difference =−0.5833, 95% CI −1.117 to −0.04932), cerebellum =0.0134 (mean difference −0.8182, 95% CI −1.473 to −0.1630), cerebellum/brainstem =0.0003 (mean difference =−1.038, 95% CI −1.584 to −0.4916), wild type untreated vs *Ndufs4*$^{-/-}$ acarbose-treated, thalamus/hippocampus =0.0031 (mean difference =−0.9167, 95% CI −1.488 to −0.3457). N = 12/group wild type and *Ndufs4*$^{-/-}$ untreated, N = 7 *Ndufs4*$^{-/-}$ acarbose-treated. **d**. Western blot and **e**. densitometric analysis of Trem-2 expression in 50 days old brain lysates from wild type untreated (dark blue), *Ndufs4*$^{-/-}$ untreated (light blue), and acarbose-treated *Ndufs4*$^{-/-}$ mice (red). Bars are mean +/− standard deviation. N = 4/group, One-way ANOVA.

https://doi.org/10.1038/s42255-023-00815-w

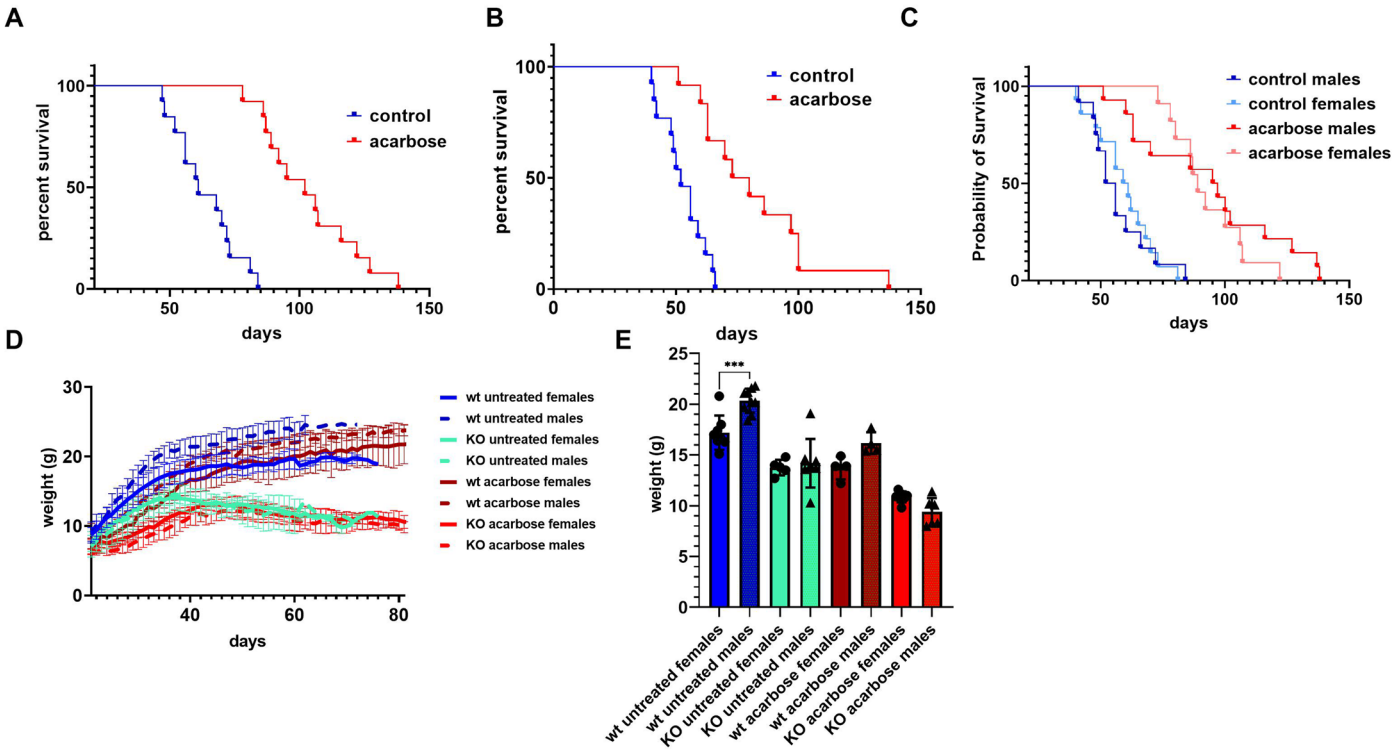

Extended Data Fig. 2 | Acarbose effects are independent of sex. A. and B. Individual survival curves of control-chow and acarbose-chow fed *Ndufs4*$^{-/-}$ mice. A. Log-rank $p < 0.0001$ N = 13/group B. Log-rank $p < 0.001$ N = 13 untreated, N = 12 acarbose-treated C. Pooled lifespan curves divided by sex. Log-rank $p < 0.5944$, N = 14 acarbose-treated males, N = 11 acarbose-treated females. D. Weight progression from weaning until post-natal day 81. Solid dark blue: female wild type mice fed control chow. Dotted dark blue: male wild type mice fed control chow. Solid dark red: female wild type mice fed acarbose chow. Dotted dark red: male wild type mice fed acarbose chow. Solid light blue: female *Ndufs4*$^{-/-}$ mice fed control chow Dotted light blue: male *Ndufs4*$^{-/-}$ mice fed control chow. Solid light red: female *Ndufs4*$^{-/-}$ mice fed acarbose chow. Dotted light red: male *Ndufs4*$^{-/-}$ mice fed acarbose chow. N = 8 female wild type untreated, N = 9 male wild type untreated, N = 5 females *Ndufs4*$^{-/-}$ untreated, N = 7 males *Ndufs4*$^{-/-}$ untreated, N = 4 females wild type acarbose, N = 4 males wild type acarbose, N = 7 females *Ndufs4*$^{-/-}$ acarbose, N = 6 males *Ndufs4*$^{-/-}$ acarbose. E. Comparison of weights at 35 days post-natal for control-chow fed wild type, *Ndufs4*$^{-/-}$ mice, acarbose-chow fed wild type, and *Ndufs4*$^{-/-}$ mice, divided by sex. *** $p < 0.001$ one way ANOVA. N = 8 female wild type untreated, N = 9 male wild type untreated, N = 5 females *Ndufs4*$^{-/-}$ untreated, N = 7 males *Ndufs4*$^{-/-}$ untreated, N = 4 females wild type acarbose, N = 4 males wild type acarbose, N = 7 females *Ndufs4*$^{-/-}$ acarbose, N = 6 males *Ndufs4*$^{-/-}$ acarbose.

https://doi.org/10.1038/s42255-023-00815-w

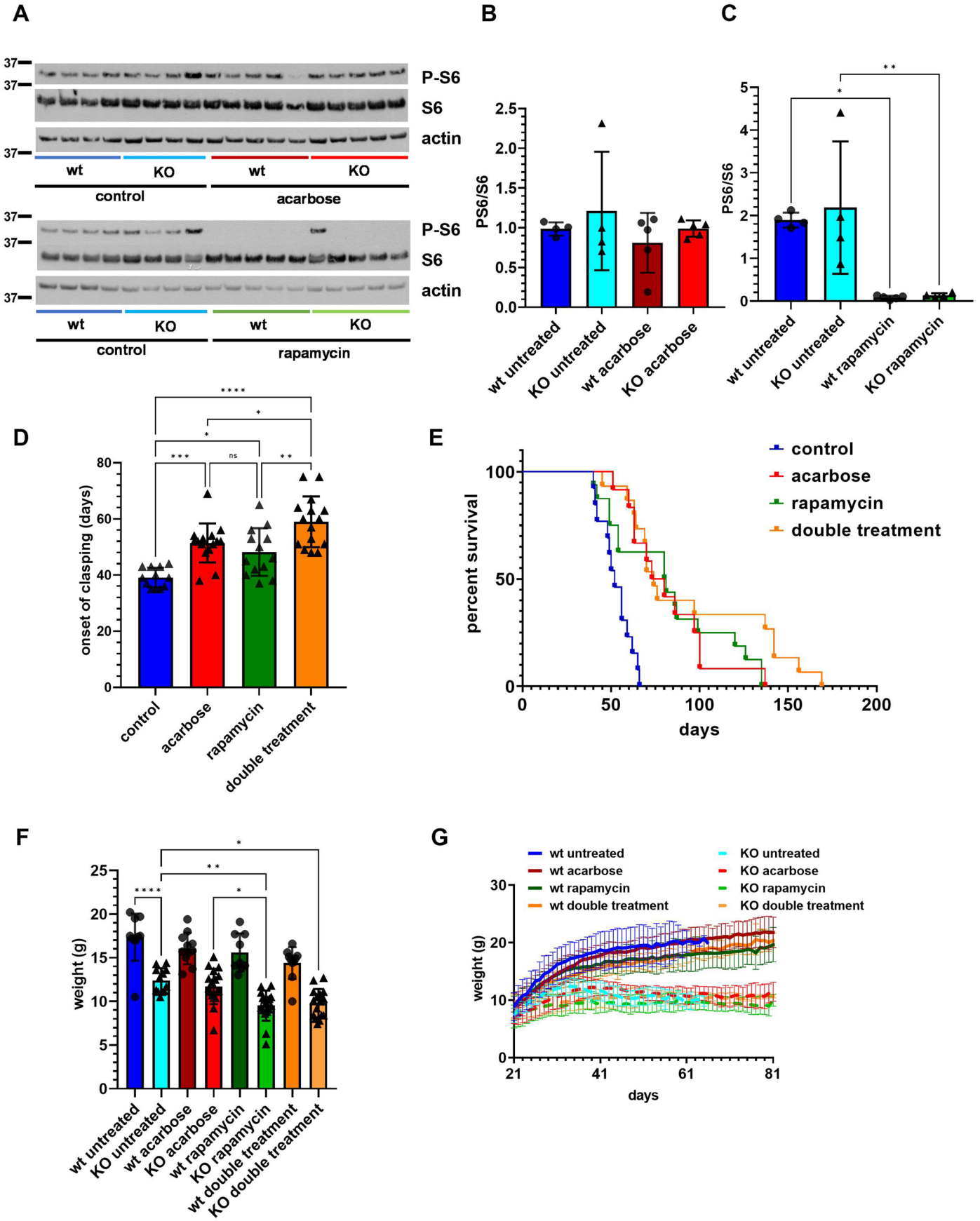

Extended Data Fig. 3 | See next page for caption.

https://doi.org/10.1038/s42255-023-00815-w

Extended Data Fig. 3 | Acarbose does not inhibit mTORc1 signaling but does not further extend lifespan in *Ndufs4*$^{-/-}$ mice treated with rapamycin. **a**. Western blots of ribosomal protein S6 phosphorylation at serine 235/236. **b. c**. Densitometric analysis of the western blots in panel A. Data are mean +/− standard deviation. One-way ANOVA adjusted p-values: wild type untreated vs. wild type rapamycin =0.0148 (mean difference =1.813, 95% CI 0.3369 to 3.289), *Ndufs4*$^{-/-}$ untreated vs *Ndufs4*$^{-/-}$ rapamycin treated =0.0092 (mean difference= 2.048. 95% CI 0.4927 to 3.604). N = 4 wild type and *Ndufs4*$^{-/-}$ untreated, N = 5 wild type and *Ndufs4*$^{-/-}$ acarbose or rapamycin treated. **d**. Onset of neurological symptoms (clasping) measured in days after birth in control-chow (blue,) 0.1% acarbose-chow (red) fed, 8 mg/kg/day I.P. rapamycin-treated (green,) acarbose-chow fed and every other day rapamycin treated (orange) *Ndufs4*$^{-/-}$ mice. Data are mean +/− standard deviation. One-way ANOVA adjusted p-values: *Ndufs4*$^{-/-}$ untreated vs acarbose-treated =0.0005 (mean difference −12.32, 95% CI −19.97 to −4.667), *Ndufs4*$^{-/-}$ untreated vs. rapamycin-treated =0.0186 (mean difference =−9.071, 95% CI −16.98 to −1.163), *Ndufs4*$^{-/-}$ untreated vs double-treated <0.0001 (mean difference = −19.85, 95% CI −27.50 to −12.20), acarbose-treated *Ndufs4*$^{-/-}$ vs double treated =0.0375 (mean difference =−7.533, 95% CI −14.75 to −0.3207), rapamycin-treated *Ndufs4*$^{-/-}$ vs double treated =0.0020 (mean difference =−10.78, 95% CI −18.26 to −3.295). N = 12 *Ndufs4*$^{-/-}$ untreated, N = 15 *Ndufs4*$^{-/-}$ acarbose, N = 13 *Ndufs4*$^{-/-}$ rapamycin, N = 15 *Ndufs4*$^{-/-}$ double treated **e**. Survival curves of *Ndufs4*$^{-/-}$ mice fed either control (blue,) 0.1% acarbose diet (red,) treated with 8 mg/kg daily intraperitoneal rapamycin (orange,) acarbose diet + every other day rapamycin (orange). Median lifespan was 52 days for control-chow fed, 76.5 days for acarbose-chow fed mice (log-rank p < 0.05), 80 for rapamycin treated mice (log-rank p < 0.05), and 74 for double treatment regimens (log-rank p < 0.01). Double treatment with acarbose and every other day rapamycin also increased maximum lifespan, Mann-Whitney U, p < 0.05. N = 13 *Ndufs4*$^{-/-}$ untreated, N = 12 *Ndufs4*$^{-/-}$ acarbose, N = 16 *Ndufs4*$^{-/-}$ rapamycin, N = 15 *Ndufs4*$^{-/-}$ double treated **f**. Comparison of body weight progression at 35 days post-natal for untreated wt (dark blue), untreated *Ndufs4*$^{-/-}$ (light blue), acarbose treated wt (dark red), acarbose treated *Ndufs4*$^{-/-}$ (light red), rapamycin treated wt (dark green), rapamycin treated *Ndufs4*$^{-/-}$ (light green), double treated wt (dark orange), and double treated *Ndufs4*$^{-/-}$ mice (light orange). One-way ANOVA adjusted p-values: wild type untreated vs *Ndufs4*$^{-/-}$ untreated <0.0001 (mean difference =4.958, 95% CI 2.436 to 7.480), *Ndufs4*$^{-/-}$ untreated vs rapamycin-treated =0.0029 (mean difference =2.880, 95% CI 0.6592 to 5.101), *Ndufs4*$^{-/-}$ untreated vs double-treated =0.0119 (mean difference = 2.604, 95% CI 0.3549 to 4.853), acarbose-treated *Ndufs4*$^{-/-}$ vs rapamycin-treated =0.0229 (mean difference =2.199. 95% CI 0.1792 to 4.220). N = 10 wild type untreated, N = 13 *Ndufs4*$^{-/-}$ untreated, N = 11 wild type acarbose-treated, N = 17 *Ndufs4*$^{-/-}$ acarbose-treated, N = 9 wild type rapamycin-treated, N = 16 *Ndufs4*$^{-/-}$ rapamycin-treated, N = 10 wild type double treated, N = 15 *Ndufs4*$^{-/-}$ double treated, sex: both. **G**. Weight progression from weaning until post-natal day 81. Solid dark blue: wild type mice fed control chow. Solid dark red: wild type mice fed acarbose chow. Dotted light blue: *Ndufs4*$^{-/-}$ mice fed control chow. Dotted light red: *Ndufs4*$^{-/-}$ mice fed acarbose chow. Solid dark green: wt rapamycin. Dotted light green: *Ndufs4*$^{-/-}$ rapamycin. Solid dark orange: wt double treated. Dotted light orange: *Ndufs4*$^{-/-}$ double treated. N = 10 wild type untreated, N = 13 *Ndufs4*$^{-/-}$ untreated, N = 11 wild type acarbose-treated, N = 17 *Ndufs4*$^{-/-}$ acarbose-treated, N = 9 wild type rapamycin-treated, N = 16 *Ndufs4*$^{-/-}$ rapamycin-treated, N = 10 wild type double treated, N = 15 *Ndufs4*$^{-/-}$ double treated, sex: both.

https://doi.org/10.1038/s42255-023-00815-w

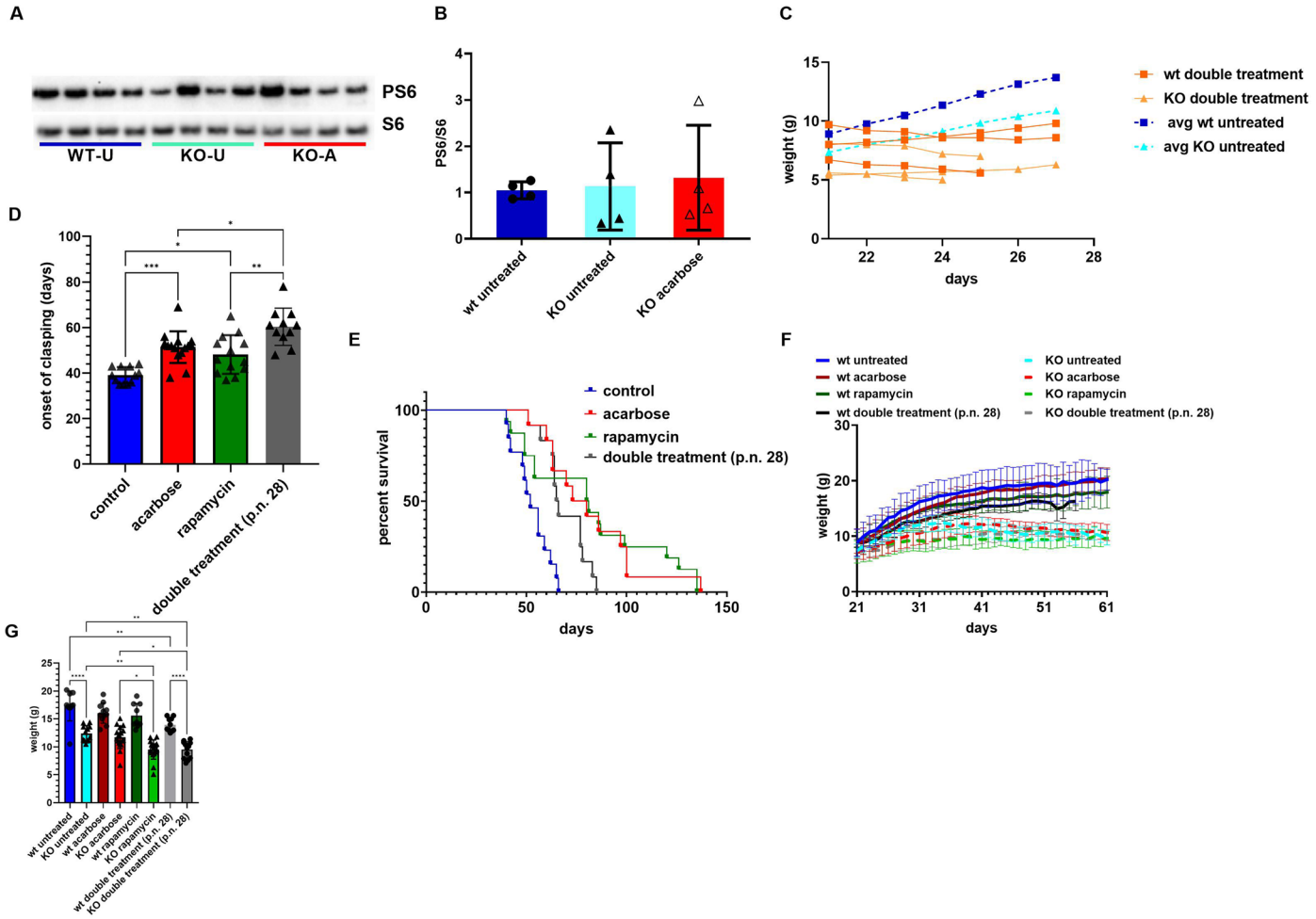

Extended Data Fig. 4 | Combination therapy with acarbose and rapamycin in *Ndufs4*$^{-/-}$ mice. A. Western blot and **B**. densitometric analysis of ribosomal protein S6 phosphorylation in brains from 50 days old wild type untreated, *Ndufs4*$^{-/-}$ untreated, and acarbose treated *Ndufs4*$^{-/-}$ mice. Data are mean +/− standard deviation N = 4/group, One-way ANOVA. **C**. Daily double treatment with acarbose and rapamycin prevents growth and ultimately causes death in newly weaned mice. Solid lines indicate weight progression individual animals on daily double treatment with rapamycin and acarbose from weaning. Dark orange squares: wild type animals, light orange triangles: *Ndufs4*$^{-/-}$ animals Dotted lines are average weights of untreated animals, dark blue squares: wild type untreated, light blue triangles, *Ndufs4*$^{-/-}$ untreated. **D**. Onset of neurological symptoms (clasping) measured in days after birth in control-chow (blue,) 0.1% acarbose-chow (red) fed, 8 mg/kg/day I.P. rapamycin-treated (green,) acarbose-chow fed from weaning and daily rapamycin treated from post natal (p.n.) day 28 (grey) *Ndufs4*$^{-/-}$ mice. Data are mean +/− standard deviation. One-way ANOVA adjusted p-values: *Ndufs4*$^{-/-}$ untreated vs acarbose-treated =0.0004 (mean difference −12.32, 95% CI −20.08 to −4.550), *Ndufs4*$^{-/-}$ untreated vs. rapamycin-treated =0.0196 (mean difference =−9.071, 95% CI −17.10 to −10.43), *Ndufs4*$^{-/-}$ untreated vs double-treated <0.0001 (mean difference = −21.28, 95% CI −29.65 to −12.91), acarbose-treated *Ndufs4*$^{-/-}$ vs double treated =0.0202 (mean difference =−8.964, 95% CI −16.92 to −1.004), rapamycin-treated *Ndufs4*$^{-/-}$ vs double treated =0.0011 (mean difference =−12.21, 95% CI −20.42 to −3.995). N = 12 *Ndufs4*$^{-/-}$ untreated, N = 15 *Ndufs4*$^{-/-}$ acarbose, N = 13 *Ndufs4*$^{-/-}$ rapamycin, N = 11 *Ndufs4*$^{-/-}$ double treated. **E**. Survival curves of *Ndufs4*$^{-/-}$ mice fed either control (blue), 0.1% acarbose diet (red), treated with 8 mg/kg daily intraperitoneal rapamycin (orange), acarbose diet + every other day rapamycin (orange). Median lifespan was 52 days for control-chow fed, 76.5 days for acarbose-chow fed mice (log-rank p < 0.05), 80 for rapamycin treated mice (log-rank p < 0.05), and 74 for double treatment regimens (log-rank p < 0.01). Double treatment with acarbose and every other day rapamycin also increased maximum lifespan, Mann-Whitney U, p < 0.05. N = 13 *Ndufs4*$^{-/-}$ untreated, N = 12 *Ndufs4*$^{-/-}$ acarbose, N = 16 *Ndufs4*$^{-/-}$ rapamycin, N = 15 *Ndufs4*$^{-/-}$ double treated **F**. Comparison of body weight progression at 35 days post-natal for untreated wt (dark blue), untreated *Ndufs4*$^{-/-}$ (light blue), acarbose treated wt (dark red), acarbose treated *Ndufs4*$^{-/-}$ (light red), rapamycin treated wt (dark green), rapamycin treated *Ndufs4*$^{-/-}$ (light green), double treated wt (dark orange), and double treated *Ndufs4*$^{-/-}$ mice (light orange). One-way ANOVA adjusted p-values: wild type untreated vs *Ndufs4*$^{-/-}$ untreated <0.0001 (mean difference = 4.958, 95% CI 2.436 to 7.480), *Ndufs4*$^{-/-}$ untreated vs rapamycin-treated = 0.0029 (mean difference = 2.880, 95% CI 0.6592 to 5.101), *Ndufs4*$^{-/-}$ untreated vs double-treated = 0.0119 (mean difference = 2.604, 95% CI 0.3549 to 4.853), acarbose-treated *Ndufs4*$^{-/-}$ vs rapamycin-treated = 0.0229 (mean difference = 2.199. 95% CI 0.1792 to 4.220). N = 10 wild type untreated, N = 13 *Ndufs4*$^{-/-}$ untreated, N = 11 wild type acarbose-treated, N = 17 *Ndufs4*$^{-/-}$ acarbose-treated, N = 9 wild type rapamycin-treated, N = 16 *Ndufs4*$^{-/-}$ rapamycin-treated, N = 10 wild type double treated, N = 15 *Ndufs4*$^{-/-}$ double treated, sex: both. **G**. Weight progression from weaning until post-natal day 81. Solid dark blue: wild type mice fed control chow. Solid dark red: wild type mice fed acarbose chow. Dotted light blue: *Ndufs4*$^{-/-}$ mice fed control chow. Dotted light red: *Ndufs4*$^{-/-}$ mice fed acarbose chow. Solid dark green: wt rapamycin. Dotted light green: *Ndufs4*$^{-/-}$ rapamycin. Solid dark orange: wt double treated. Dotted light orange: *Ndufs4*$^{-/-}$ double treated. N = 10 wild type untreated, N = 13 *Ndufs4*$^{-/-}$ untreated, N = 11 wild type acarbose-treated, N = 17 *Ndufs4*$^{-/-}$ acarbose-treated, N = 9 wild type rapamycin-treated, N = 16 *Ndufs4*$^{-/-}$ rapamycin-treated, N = 10 wild type double treated, N = 15 *Ndufs4*$^{-/-}$ double treated, sex: both.

https://doi.org/10.1038/s42255-023-00815-w

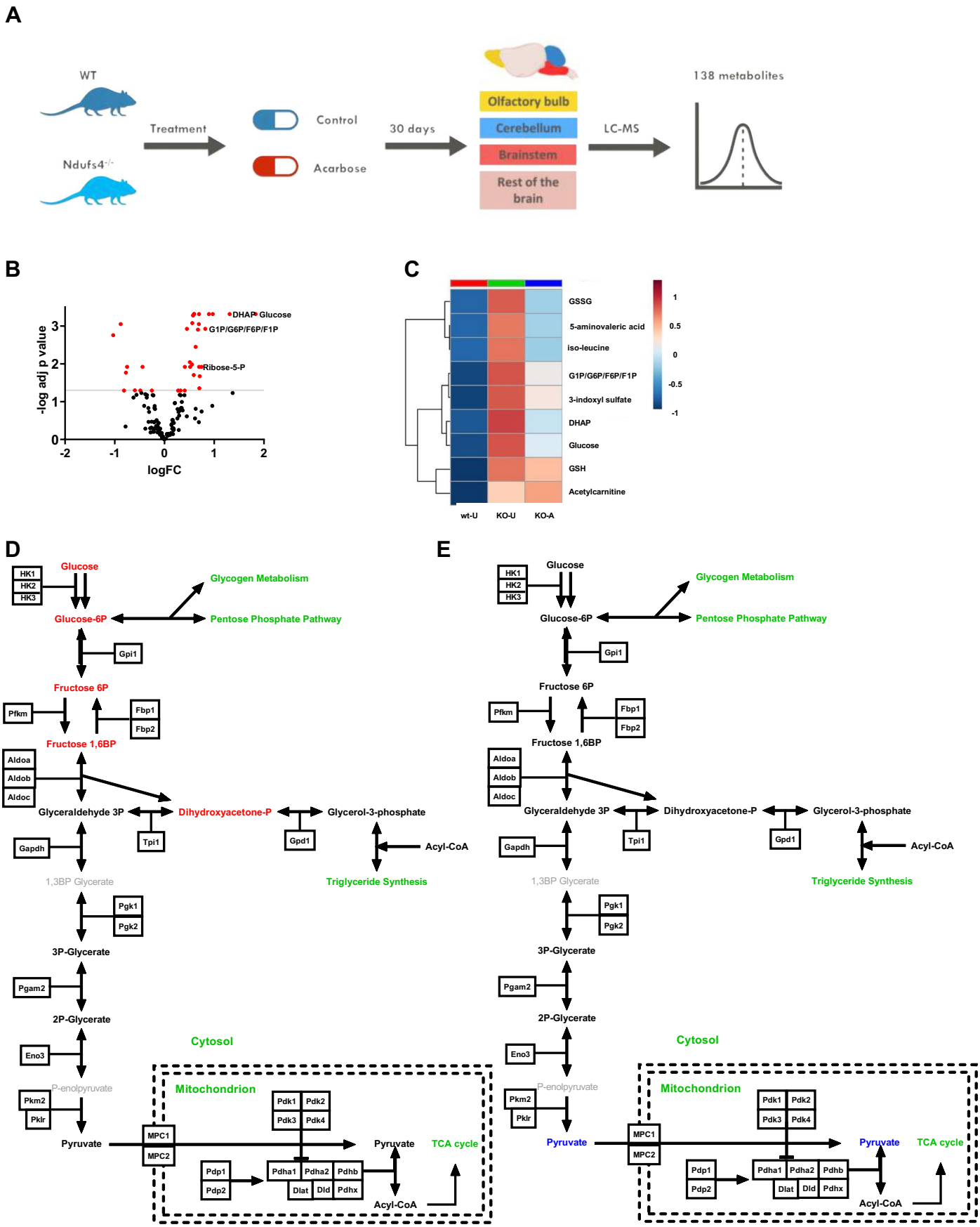

Extended Data Fig. 5 | See next page for caption.

https://doi.org/10.1038/s42255-023-00815-w

Extended Data Fig. 5 | Metabolic profiling of brain regions in *Ndufs4*$^{-/-}$ mice treated with acarbose. a. Schematic diagram of the metabolomics assay. **b**. Volcano plot of metabolic features in the olfactory bulb of untreated *Ndufs4*$^{-/-}$ mice compared to wild type littermates. Red dots are significantly altered metabolites. Linear model adjusted p-value (Benjamini-Hochberg FDR correction) <0.05. Individual metabolites p-values available in metabolomics dataset. **c**. Heat map of the relative abundance of selected significantly altered metabolites in the olfactory bulb of wild type untreated (WT-U), *Ndufs4*$^{-/-}$ untreated (KO-U), and acarbose-treated *Ndufs4*$^{-/-}$ mice (KO-A). **d**. and **e**. Specific Pathway Analysis of glycolysis intermediates in the olfactory bulb of untreated (D.) and acarbose-treated (E.) *Ndufs4*$^{-/-}$ mice. Red metabolites are significantly more abundant compared to untreated wild type; blue metabolites are significantly less abundant. Linear model adjusted p-value (Benjamini-Hochberg FDR correction) <0.05. Individual metabolites p-values available in metabolomics dataset. N = 4-5 per group.

https://doi.org/10.1038/s42255-023-00815-w

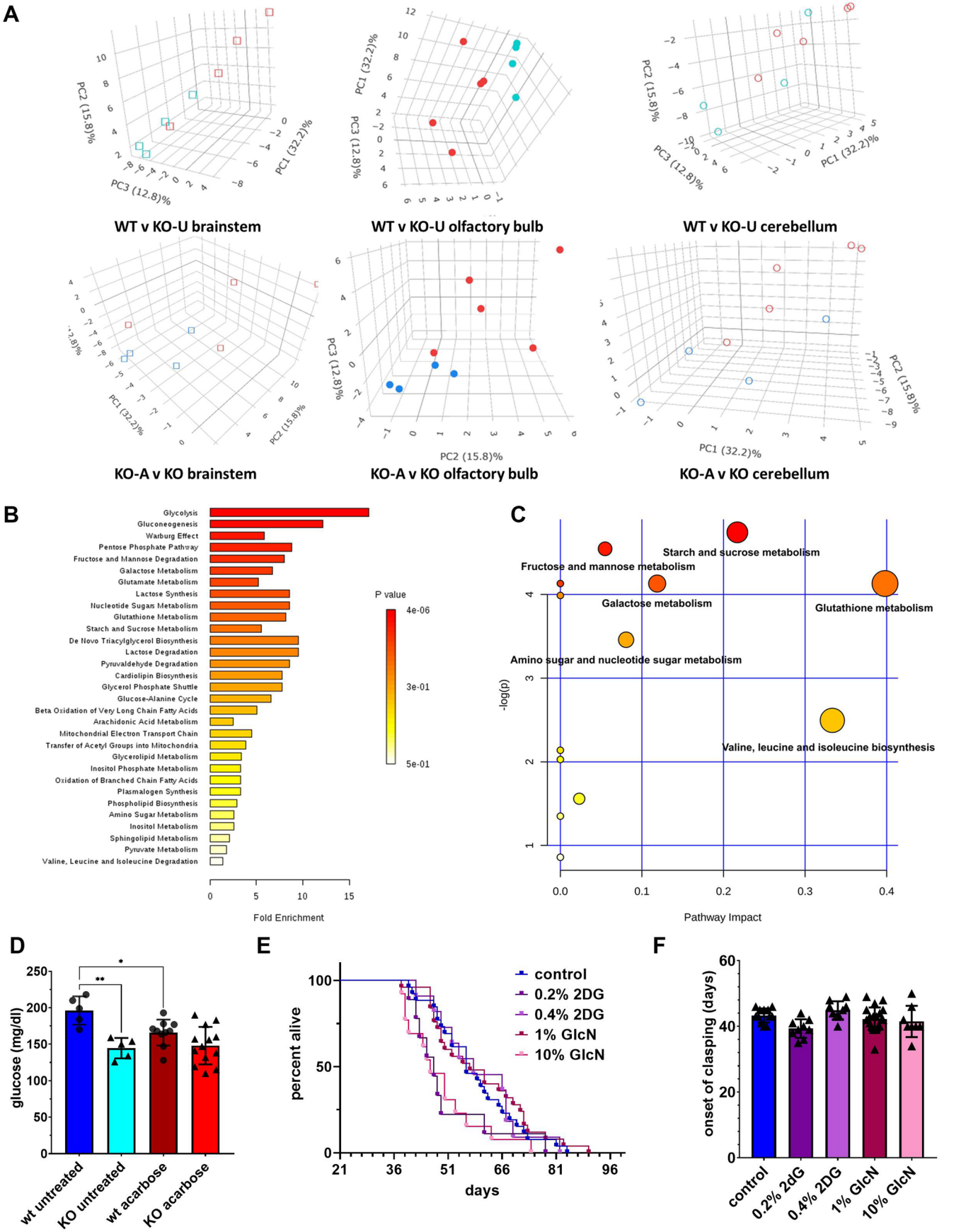

Extended Data Fig. 6 | See next page for caption.

https://doi.org/10.1038/s42255-023-00815-w

Extended Data Fig. 6 | Metabolomics reveals glucose dishomeostasis in *Ndufs4*$^{-/-}$ brains. a Principal component analysis of the metabolomics dataset described in Fig. 4a. Light blue squares and circles, wild type untreated; red squares and circles, *Ndufs4*$^{-/-}$ untreated; dark blue squares and circles, acarbose-treated *Ndufs4*$^{-/-}$. **b**. Metabolites Set Enrichment Analysis (MSEA) of metabolic pathways enriched in the olfactory bulb of untreated *Ndufs4*$^{-/-}$ compared to wild type animals. **c**. Metabolites Pathway Analysis (MPA) of metabolic pathways enriched in the olfactory bulb of untreated *Ndufs4*$^{-/-}$ compared to wild type animals. Color denotes p-value, same scale as in panel B., size of circles denotes impact. N = 4-5 per group for panels A to C. **d**. 1 h post-prandial blood glucose levels in wild type and *Ndufs4*$^{-/-}$ mice untreated or treated with acarbose. Data are mean +/− standard deviation. One-way ANOVA adjusted p-values: wild type untreated vs. *Ndufs4*$^{-/-}$ untreated =0.0018 (mean difference= 51.6, 95% CI 17.64 to 85.56), wild type untreated vs wild type acarbose =0.0428 (mean difference =30.2, 95% CI 0.7883 to 59.61). N = 5 wild type and *Ndufs4*$^{-/-}$ untreated, N = 10 wild type N = 13 *Ndufs4*$^{-/-}$ acarbose-treated. **e**. Survival plot of *Ndufs4*$^{-/-}$ mice treated with 0.2%, 0.4% 2-deoxyglucose (2DG) or 1%, 10% glucosamine (GlcN) mixed in the food. N = 26 untreated, N = 9 0.2% 2-deoxyglucose, N = 11 0.4% 2-deoxyglucose, N = 25 1% glucosamine, N = 13 10% glucosamine. **F**. Onset of clasping in *Ndufs4*$^{-/-}$ mice treated with 2-deoxyglucose (2DG) or glucosamine (GlcN). Data are mean +/− standard deviation. N = 12 untreated, N = 9 0.2% and 0.4% deoxyglucose, N = 21 1% glucosamine, N = 8 10% glucosamine.

https://doi.org/10.1038/s42255-023-00815-w

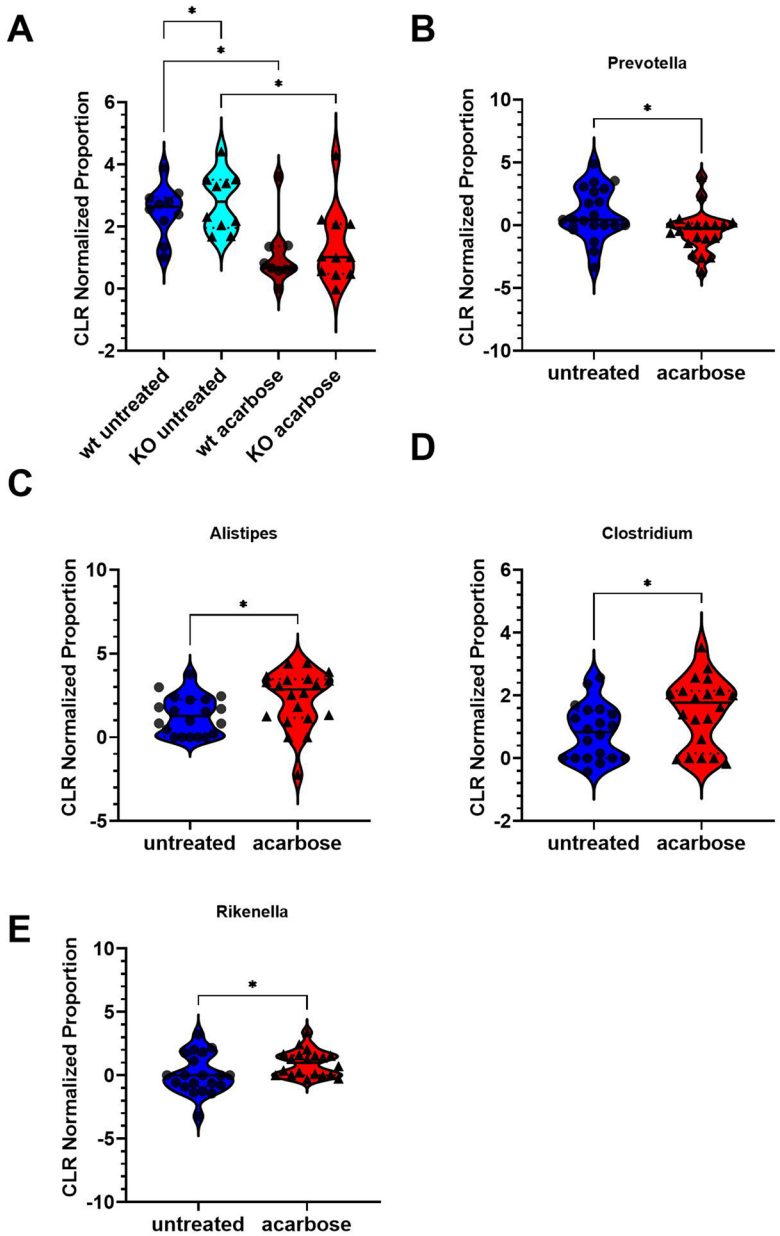

Extended Data Fig. 7 | Acarbose alters the intestinal microbiome in *Ndufs4*$^{-/-}$ mice. a. Centered log-ratio normalized proportion of Bacteroides divided by genotype and treatment. Linear regression p-value by treatment adjusted by genotype =0.001. N = 9-11 per group **b-e**. Center log-ratio normalized proportion of Prevotella (B.) Alistipes (C.) Clostridium (D.) and Rikenella (E.) divided by treatment. Linear regression p-value by treatment= 0.023 (B), 0.026 (C), 0.036 (D), 0.038 (E), FDR = 0.136.

https://doi.org/10.1038/s42255-023-00815-w

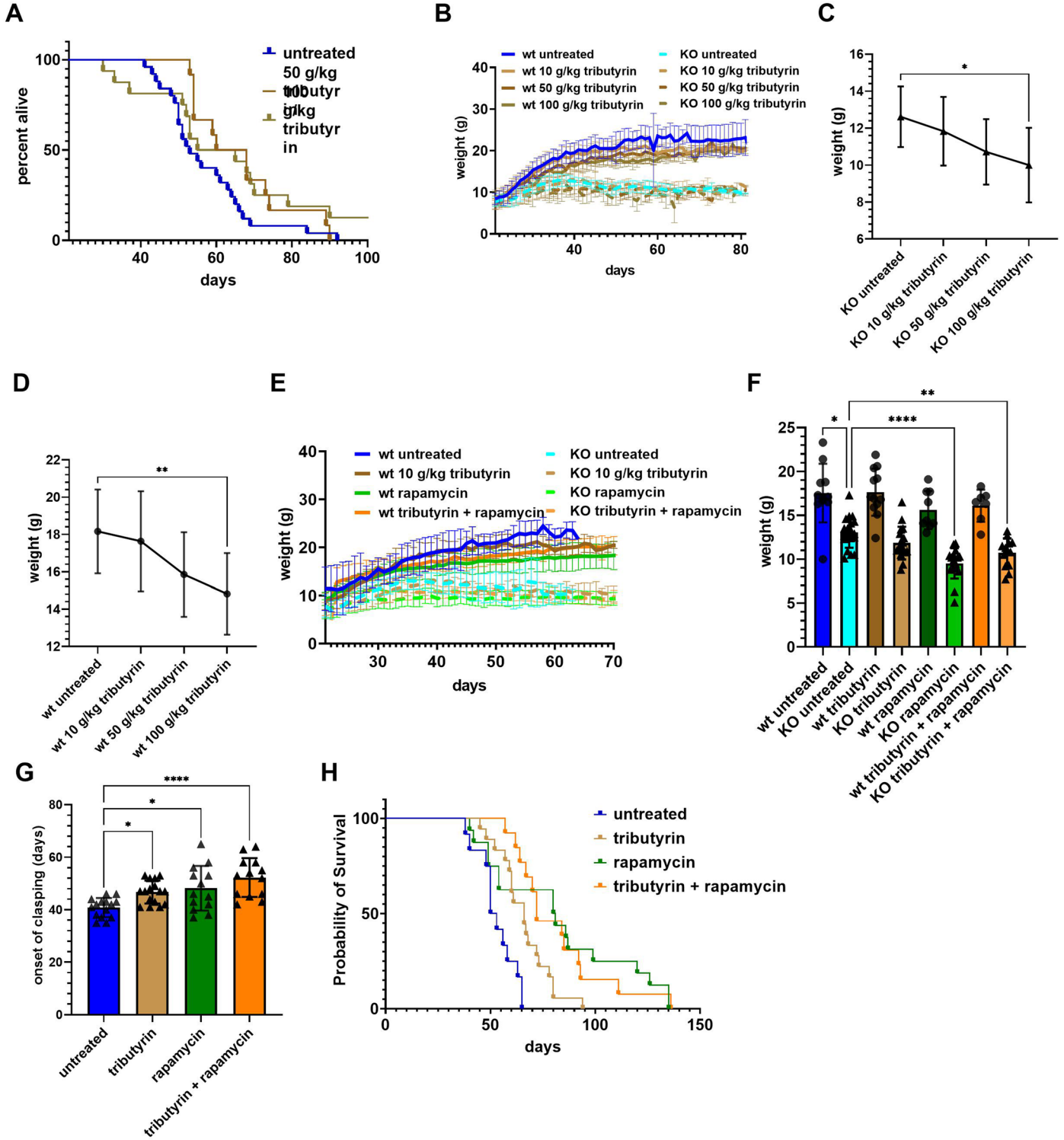

Extended Data Fig. 8 | See next page for caption.

https://doi.org/10.1038/s42255-023-00815-w

Extended Data Fig. 8 | Tributyrin supplementation improves survival in *Ndufs4*$^{-/-}$ mice. a. Survival plot of *Ndufs4*$^{-/-}$ treated with 50 mg/kg or 100 g/kg tributyrin. N = 25 untreated, N = 12 50 g/kg tributyrin, N = 16 100 g/kg tributyrin. **b**. Weight progression from weaning until post-natal day 81. Solid dark blue: wild type mice fed control chow (dark blue), *Ndufs4*$^{-/-}$ untreated (light blue), and tributyrin (shades of brown). Data are mean +/− standard deviation. N = 13 wild type and *Ndufs4*$^{-/-}$ untreated, N = 12 wild type 10 g/kg tributyrin, N = 18 *Ndufs4*$^{-/-}$ 10 g/kg tributyrin, N = 13 wild type and *Ndufs4*$^{-/-}$ 50 g/kg tributyrin, N = 12 wild type 100 g/kg tributyrin, N = 15 100 g/kg tributyrin. N = 20/group **c**-**d**. Linear trend of *Ndufs4*$^{-/-}$ (C.) and wild type mice (D.) weight after treatment with increasing doses of tributyrin at post-natal day 35. Data are mean +/− standard deviation. One-way ANOVA test for linear trend p-value = 0.0003 (*Ndufs4*$^{-/-}$), 0.0005 (wild type). N = 13 wild type and *Ndufs4*$^{-/-}$ untreated, N = 12 wild type 10 g/kg tributyrin, N = 18 *Ndufs4*$^{-/-}$ 10 g/kg tributyrin, N = 13 wild type and *Ndufs4*$^{-/-}$ 50 g/kg tributyrin, N = 12 wild type 100 g/kg tributyrin, N = 15 100 g/kg tributyrin. **e**. Weight progression from weaning until post-natal day 70. Solid: wild type mice, dotted: *Ndufs4*$^{-/-}$ mice fed control chow (blue), tributyrin (brown), or rapamycin (green). Data are mean +/− standard deviation. **f**. Comparison of weights at 35 days post-natal for wild type and *Ndufs4*$^{-/-}$ fed either chow (blue), chow supplemented with 10 g/kg tributyrin (brown), injected with rapamycin (green), or fed chow supplemented with 10 g/kg tributyrin and injected with rapamycin (orange). Data are mean +/− standard deviation. One-way ANOVA, adjusted p-values: wt untreated vs *Ndufs4*$^{-/-}$ untreated =0.0112 (mean difference 4.5, 95% CI 0.8824 to 8.119), *Ndufs4*$^{-/-}$ untreated vs. *Ndufs4*$^{-/-}$ rapamycin-treated <0.0001 (mean difference 3.533, 95% CI 1.807 to 5.260), *Ndufs4*$^{-/-}$ untreated vs *Ndufs4*$^{-/-}$ tributyrin+rapamycin-treated =0.007 (mean difference 2.330, 95% CI 0.4753 to 4.184). N = 11 wild type untreated, N = 21 *Ndufs4*$^{-/-}$ untreated, N = 12 wild type 10 g/kg tributyrin, N = 18 *Ndufs4*$^{-/-}$ 10 g/kg tributyrin, N = 9 wt rapamycin, N = 17 *Ndufs4*$^{-/-}$ rapamycin, N = 7 wt tributyrin + rapamycin, N = 13 *Ndufs4*$^{-/-}$ tributyrin + rapamycin. **g**. Onset of clasping in untreated (blue), tributyrin-treated (brown), rapamycin treated (green), or tributyrin and rapamycin-treated *Ndufs4*$^{-/-}$ mice. Data are mean +/− standard deviation. One-way ANOVA, adjusted p-value untreated vs tributyrin =0.0486 (mean difference −5.888, 95% CI −11.75 to −0.02388), untreated vs. rapamycin =0.0126 (mean difference =−7.354, 95% CI −13.54 to −1.172), untreated vs. tributyrin+rapamycin <0.0001 (mean difference = −11.43, 95% CI −17.61 to −5.248). N = 15 untreated, N = 16 tributyrin-treated, N = 13 rapamycin-treated, N = 13 tributyrin and rapamycin treated. **h**. Survival plot of *Ndufs4*$^{-/-}$ untreated (blue), tributyrin-treated (brown), rapamycin treated (green), or tributyrin and rapamycin-treated *Ndufs4*$^{-/-}$ mice. N = 12 untreated, N = 18 tributyrin, N = 16 rapamycin, N = 13 tributyrin + rapamycin. Log-rank p<0.0001.

https://doi.org/10.1038/s42255-023-00815-w

Extended Data Table 1 | Short-Chain Fatty Acids Panel

SPQC SCFA	Average (nmol/mg)	CV %
Acetic acid	2.73E+01	0.44%
Propionic acid	4.93E+00	1.70%
iso-butyric acid	1.63E-01	1.89%
butyric acid	2.58E+00	1.75%
2-methyl butyric acid	5.03E-02	0.54%
iso-valeric acid	5.07E-02	2.00%
valeric acid	2.15E-01	0.92%
3-methyl valeric acid	BLOQ	BLOQ
iso-caproic acid	BLOQ	BLOQ
caproic acid	4.96E-03	9.56%
Heptanoic acid	BLOQ	BLOQ
Octanoic acid	BLOQ	BLOQ

Short Chain Fatty Acids monitored via LC-MS and their average detection level in mouse ceca.

nature portfolio

Corresponding author(s): Matt Kaeberlein

Last updated by author(s): Apr 12, 2023

Reporting Summary

Nature Portfolio wishes to improve the reproducibility of the work that we publish. This form provides structure for consistency and transparency in reporting. For further information on Nature Portfolio policies, see our Editorial Policies and the Editorial Policy Checklist.

Statistics

For all statistical analyses, confirm that the following items are present in the figure legend, table legend, main text, or Methods section.

n/a	Confirmed
☐	☒ The exact sample size (*n*) for each experimental group/condition, given as a discrete number and unit of measurement
☐	☒ A statement on whether measurements were taken from distinct samples or whether the same sample was measured repeatedly
☐	☒ The statistical test(s) used AND whether they are one- or two-sided *Only common tests should be described solely by name; describe more complex techniques in the Methods section.*
☒	☐ A description of all covariates tested
☐	☒ A description of any assumptions or corrections, such as tests of normality and adjustment for multiple comparisons
☐	☒ A full description of the statistical parameters including central tendency (e.g. means) or other basic estimates (e.g. regression coefficient) AND variation (e.g. standard deviation) or associated estimates of uncertainty (e.g. confidence intervals)
☐	☒ For null hypothesis testing, the test statistic (e.g. *F*, *t*, *r*) with confidence intervals, effect sizes, degrees of freedom and *P* value noted *Give P values as exact values whenever suitable.*
☒	☐ For Bayesian analysis, information on the choice of priors and Markov chain Monte Carlo settings
☒	☐ For hierarchical and complex designs, identification of the appropriate level for tests and full reporting of outcomes
☒	☐ Estimates of effect sizes (e.g. Cohen's *d*, Pearson's *r*), indicating how they were calculated

Our web collection on statistics for biologists contains articles on many of the points above.

Software and code

Policy information about availability of computer code

Data collection	Analyst 1.5
Data analysis	GraphPad 9.3.1, USEARCH7, Skyline v2.1.1.1, R 4.0.2, Visiopharm 22.03.0.11565

For manuscripts utilizing custom algorithms or software that are central to the research but not yet described in published literature, software must be made available to editors and reviewers. We strongly encourage code deposition in a community repository (e.g. GitHub). See the Nature Portfolio guidelines for submitting code & software for further information.

Data

Policy information about availability of data

All manuscripts must include a data availability statement. This statement should provide the following information, where applicable:

- Accession codes, unique identifiers, or web links for publicly available datasets
- A description of any restrictions on data availability
- For clinical datasets or third party data, please ensure that the statement adheres to our policy

All source data will be uploaded with the manuscript and/or made available in a public repository upon publication

Research involving human participants, their data, or biological material

Policy information about studies with human participants or human data. See also policy information about sex, gender (identity/presentation), and sexual orientation and race, ethnicity and racism.

Reporting on sex and gender	*Use the terms sex (biological attribute) and gender (shaped by social and cultural circumstances) carefully in order to avoid confusing both terms. Indicate if findings apply to only one sex or gender; describe whether sex and gender were considered in study design; whether sex and/or gender was determined based on self-reporting or assigned and methods used.* *Provide in the source data disaggregated sex and gender data, where this information has been collected, and if consent has been obtained for sharing of individual-level data; provide overall numbers in this Reporting Summary. Please state if this information has not been collected.* *Report sex- and gender-based analyses where performed, justify reasons for lack of sex- and gender-based analysis.*
Reporting on race, ethnicity, or other socially relevant groupings	*Please specify the socially constructed or socially relevant categorization variable(s) used in your manuscript and explain why they were used. Please note that such variables should not be used as proxies for other socially constructed/relevant variables (for example, race/ethnicity should not be used as a proxy for socioeconomic status).* *Provide clear definitions of the relevant terms used, how they were provided (by the participants/respondents, the researchers, or third parties), and the method(s) used to classify people into the different categories (e.g. self-report, census or administrative data, social media data, etc.)* *Please provide details about how you controlled for confounding variables in your analyses.*
Population characteristics	*Describe the covariate-relevant population characteristics of the human research participants (e.g. age, genotypic information, past and current diagnosis and treatment categories). If you filled out the behavioural & social sciences study design questions and have nothing to add here, write "See above."*
Recruitment	*Describe how participants were recruited. Outline any potential self-selection bias or other biases that may be present and how these are likely to impact results.*
Ethics oversight	*Identify the organization(s) that approved the study protocol.*

Note that full information on the approval of the study protocol must also be provided in the manuscript.

Field-specific reporting

Please select the one below that is the best fit for your research. If you are not sure, read the appropriate sections before making your selection.

☒ Life sciences ☐ Behavioural & social sciences ☐ Ecological, evolutionary & environmental sciences

For a reference copy of the document with all sections, see nature.com/documents/nr-reporting-summary-flat.pdf

Life sciences study design

All studies must disclose on these points even when the disclosure is negative.

Sample size	For all experiments, sample size was determined based on previous experiments using an online power calculation software (https://www.dssresearch.com/KnowledgeCenter/toolkitcalculators/statisticalpowercalculators.aspx), and previous publications including: https://doi.org/10.1126/science.1244360, https://doi.org/10.1126/scitranslmed.3003802, and https://doi.org/10.7554/eLife.16351
Data exclusions	Data points were labeled outliers and excluded a priori from the analysis if higher/lower than two standard deviations above/below the mean. Data points were excluded according to these criteria from the following figure panels: 1E, Extended Data S3C.
Replication	Survival experiments were replicated twice. Large scale analyses (metabolomics, 16S sequencing) could not be repeated due to budgetary constraints but were sufficiently powered to account for individual variation among individuals
Randomization	Animals were randomly assigned to control or experimental groups at the moment of genotyping via arbitrary methods
Blinding	The veterinary pathologist, 16S sequencing technicians, and the mass spectrometrists for metabolomics and SCFAs analysis were blinded to experimental conditions. All other experiments were unblinded as it was impossible or impractical to blind the experimenter (e.g. loading order for western blots, treatment administration to live animals, etc.)

Reporting for specific materials, systems and methods

We require information from authors about some types of materials, experimental systems and methods used in many studies. Here, indicate whether each material, system or method listed is relevant to your study. If you are not sure if a list item applies to your research, read the appropriate section before selecting a response.

Materials & experimental systems

n/a	Involved in the study
☐	☒ Antibodies
☒	☐ Eukaryotic cell lines
☒	☐ Palaeontology and archaeology
☐	☒ Animals and other organisms
☒	☐ Clinical data
☒	☐ Dual use research of concern
☒	☐ Plants

Methods

n/a	Involved in the study
☒	☐ ChIP-seq
☒	☐ Flow cytometry
☒	☐ MRI-based neuroimaging

Antibodies

Antibodies used	phospho-S6 (Ser 235-236, cat 2211), total S6 (clone 5G10, cat 2217), TREM2 (clone D8I4C, cat 91068)
Validation	certificates of analysis will be attached to the submission

Animals and other research organisms

Policy information about studies involving animals; ARRIVE guidelines recommended for reporting animal research, and Sex and Gender in Research

Laboratory animals	mice, C57BL6/N Ndufs4+/+ (wild type) and Ndufs4-/- (KO), both sexes, 21 days post natal and up
Wild animals	no wild animals.
Reporting on sex	Sex based analyses were performed and yielded no sex-specific differences
Field-collected samples	no field collected samples
Ethics oversight	All animals experiments were reviewed and approved by the University of Washington Institutional Animal Care and Use Committee.

Note that full information on the approval of the study protocol must also be provided in the manuscript.